99 SEMESTERS OF CHEMISTRY – A PERSONAL RETROSPECTIVE ON THE MOLECULAR STATE APPROACH BY PREPARATIVE CHEMISTS

Hans BOCK

Chemistry Department, University of Frankfurt, Marie Curie-Str. 11, 60439 Frankfurt/Main, Germany; e-mail: bock@bock.anorg.chemie.uni-frankfurt.de

Received October 17, 1996
Accepted November 8, 1996

Molecular states are the real building blocks of the chemist, because the structure of a molecule can change considerably as its energy and thus its electron distribution varies within the time-domain of dynamic relaxation. The ever increasing use of measuring methods from the armory of physics to characterize molecules by their molecular state fingerprints and, above all, of computers to rationalize both their properties and their microscopic reaction pathways, provides a wealth of information for the development of chemistry. To deal with the complexity of molecular states, a qualitative model based on the topology and symmetry of their structures as well as of their energies resulting from the electron distribution over the respective effective nuclear potentials is presented and is illustrated by examples of our own efforts to elucidate molecular state properties including time-dependent dynamics, microscopic reaction pathways both in the gas phase and in solution, and the self-assembly of molecules on crystallization. In conclusion, a personal retrospective is summarized and some prospects for the future are outlined.

Key words: Molecular states; Microscopic reaction pathways; Self-assembly of molecules.

1. INTRODUCTORY REMARKS

1.1. Molecular State Discovery of White Phosphorus

Molecular states considerably enlarge the manifold of the approximately 10 million chemical compounds registered in the Chemical Abstract System on the basis of the topology of their structures, and by also specifying their energy[1]. This essential quantity is responsible for the colour of compounds as well as their photochemistry, for the structural changes of molecules during excitation as well as in redox reactions and also helps both to classify chemical species and to analytically characterize them through their molecular fingerprints.

A famous historical example involves the discovery of the element phosphorus by Henning Brand in 1669 as depicted in the fascinating picture by Joseph Wright (Fig. 1).

The alchemist Henning Brand, in an attempt to discover the magic stone for the conversion of silver to gold, evaporated golden-yellow urine to dryness, and by heating the residue containing the phosphate $Na^{\oplus}NH_4^{\oplus}HPO_4^{\ominus\ominus}$ along with organic compounds to a red glow, produced white phosphorus P_4 by carbon reduction[2]. The glaring light ob-

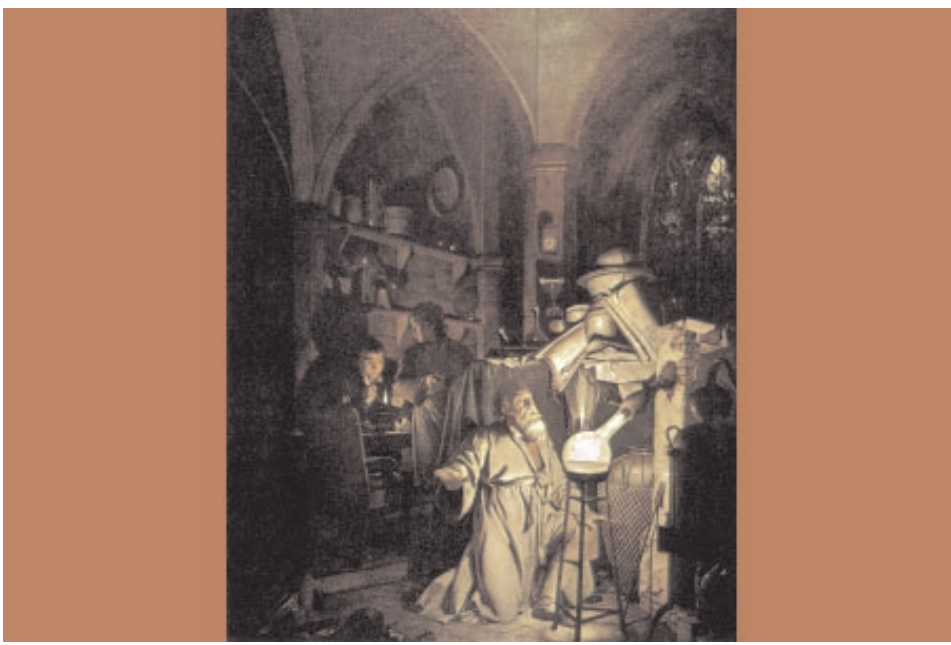

FIG. 1
The discovery of white phosphorus by H. Brand in 1669 based on the light emitted from its long-lived phosphorescent molecular state (painting by J. Wright (1734–1797); see text)

served (Fig. 1) also provided the name for the unknown element from the Greek "phosphoros" *i.e.* light carrier.

The subsequent tremendous development of chemistry to a natural science, however, has been largely dominated by breath-taking synthetic achievements[3], although important general principles and numerous measurement techniques have been established as well[3]. For instance, when the study of chemistry was begun in our group 99 semesters ago, no commercial NMR spectrometers (Nobel Prize 1952: F. Bloch and E. M. Purcell[3]) nor advanced chromatographic techniques (Nobel Prize 1952: A. J. P. Martin and R. L. M. Synge[3]) were available and, above all, transistorized computers (1972: J. S. Kilby, J. A. Hoerni and M. E. Hoff[3]) had not yet been developed. In other tremendous and breath-taking developments since then, numerous already known as well as novel measuring methods from physics, such as photoelectron spectroscopy[4] (Nobel Prize 1981: K. Siegbahn[3]) or electron spin resonance spectroscopy[5] were introduced to chemistry for more intense investigation of molecular states.

1.2. Efforts to Measure Molecular State Properties, Microscopic Reaction Pathways and Self-Assembly of Molecules

The investigations of what later became the Frankfurt Group began at the University of Munich in 1956 and in the field of preparative nitrogen chemistry (Fig. 2). The starting point was to find an efficient way to produce anhydrous hydrazine $H_2N–NH_2$, which is also used as a rocket fuel, and the exploration of its reactions[6]. Among the derivatives first synthesized was a new class of azo compounds, the violet azodiphosphonic acid derivatives[7]. Other reactive nitrogen-containing molecules investigated included the chloroamines NCl_3, $(H_3C)NCl_2$ and $(H_3C)_2NCl$, which permitted isolation of nitrogentrirhodanide[8a] $N(SCN)_3$ or dimethylamino azide[8b] $(H_3C)_2N–NNN$ and dialkylamination of benzene under Friedel–Crafts conditions[8c]. Last but not least, several doors to metal-organic nitrogen chemistry could be opened by reacting $RNCl_2$ with $Ni(CO)_4$ to yield dialkylurea[9a], $R_3P{=}NH$ with $Mo(CO)_6$ or azabutadienes $RHN{=}CH–HC{=}NHR$ with $Cr(CO)_6$ to prepare the respective metal carbonyl complexes[9b,c] or $R_2N–CN$ with $Ni(CO)_4$ to a six-membered ring trimer containing both the nitrogen electron pair $n_N \rightarrow \sigma$ and $n_N \rightarrow \pi$ coordination to the nickel centers[9d]. The stoichiometric addition of water to an otherwise anhydrous solution of $CuCl_2$ in pyridine yielded the first tetrahedral copper cluster $[(\text{pyridine}\rightarrow Cu^{\oplus\oplus})_4(Cl^{\ominus})_6(O^{\ominus\ominus})]$ with six chloride bridges and a central $O^{\ominus\ominus}$ dianion[9e]. All of these and other investigations within the area of preparative nitrogen chemistry can be summarized as "acquisition of tools", including the handling and the reactions of air-sensitive, sometimes poisonous or explosive compounds[6–9] (Fig. 1).

It was the surprising violet colour of the new azo diphosphonic acid derivatives, $R_2(O)P–N{=}N–P(O)R_2$ that widened our horizon to include molecular states by posing the question: "Why are these compounds violet?" (Fig. 3). To obtain an answer, a series

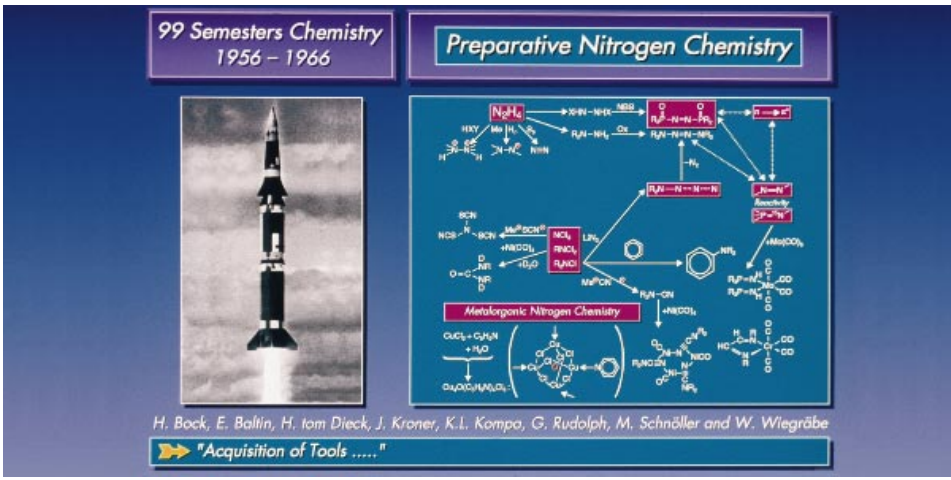

FIG. 2

Preparative nitrogen chemistry at the University of Munich, 1956 to 1966, centered around the reactions of the potential rocket-fuel anhydrous hydrazine, the properties of novel azo compounds (*cf.* Fig. 3) and of analogous phosphorus derivatives, novel products of the reactive halogen amines such as dimethylamino azide or nitrogen-trirhodanide and new metal-organic nitrogen complexes (*cf.* text)

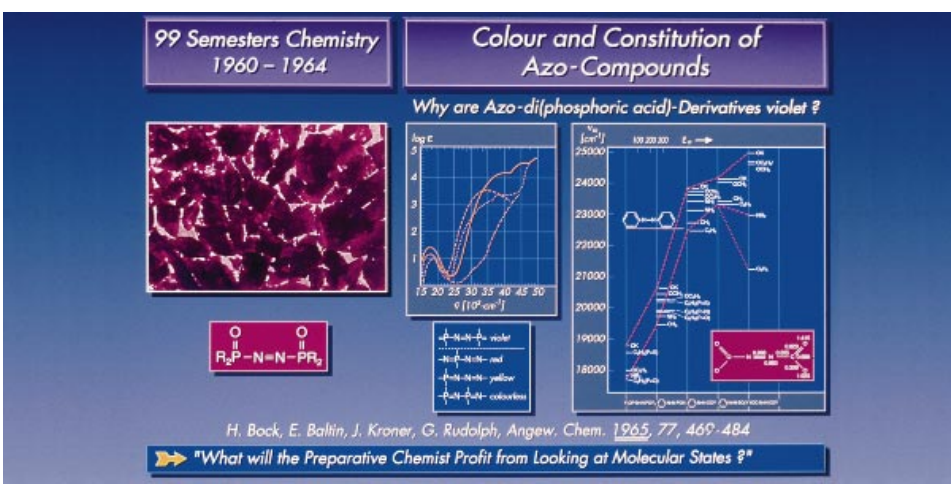

FIG. 3

Investigations 1960 to 1964 of the violet colour of crystalline tetraphenyl azodiphosphonic acid containing only a four-center P–N=N–P chromophore by UV/VIS spectra comparison with iso(valence)electronic P/N chromophores (center), other azo compounds and numerous differently substituted derivatives synthesized, along with an example (lower right) of our first π-type Hückel MO calculations (*cf.* text)

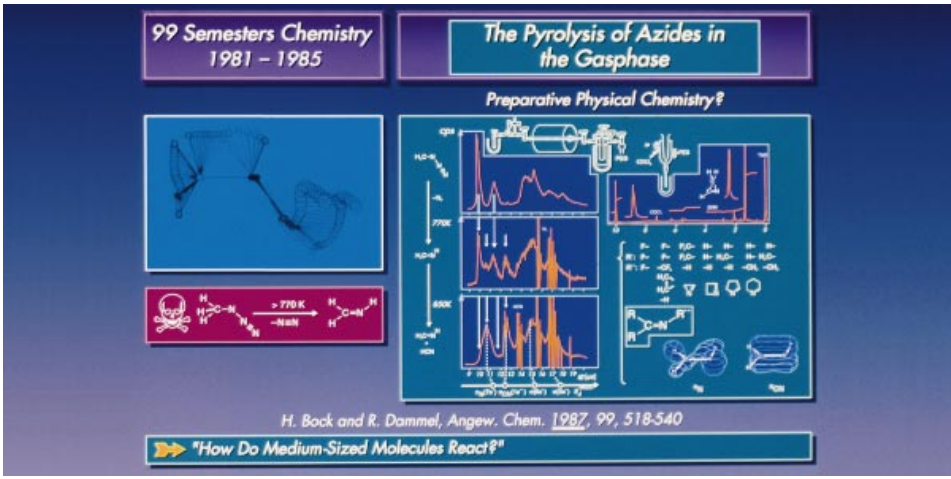

FIG. 4

Investigations 1981 to 1985 of pyrolyses of azides under unimolecular conditions in the gas phase as illustrated by the example of methyl azide with two consecutive reaction channels, $H_3C–N_3 \rightarrow H_2C=NH \rightarrow HCN$, investigated by photoelectron-spectroscopic real-time gas analysis in the apparatus shown (center), accompanied by both NMR characterization of the products (right) and a calculated hypersurface (left) discussed below (*cf.* text)

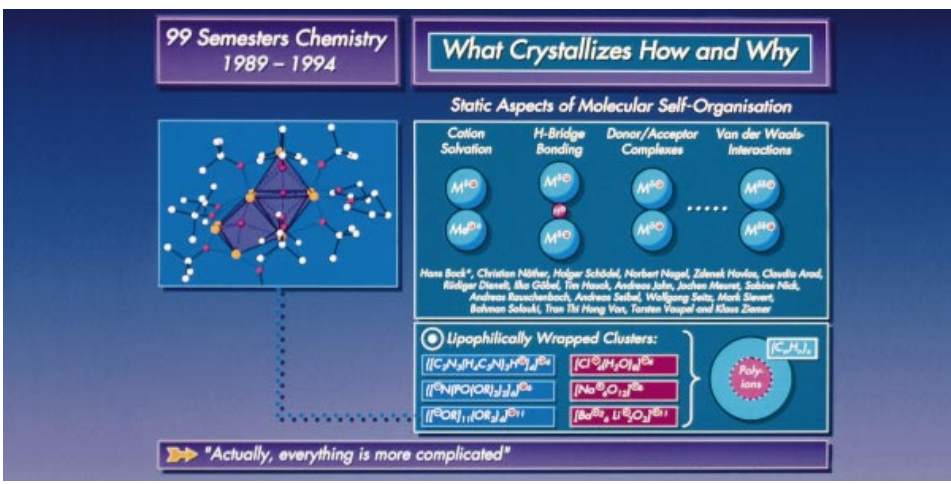

FIG. 5

Recent investigations of interactions in molecular crystals such as cation solvation, hydrogen bridge bonding, donor/acceptor complex formation or van der Waals attractions providing information on the static aspects of molecular self-organisation, studied in detail by the structural determination of lipophilically wrapped polyion aggregates discussed below (*cf.* text)

of other compounds with four-center P/N chromophores and especially with different substituents on the azo group, X(Y)Z–N=N–Z(Y)X, have been synthesized and their UV/VIS spectra compared[7]. The long-wavelength $n \rightarrow \pi^*$ transitions of low intensity as well as the intense $\pi \rightarrow \pi^*$ transitions of higher energy both exhibited characteristic shifts (Fig. 3), which could be explained by first and second order substituent (XYZ) perturbation increments. In summary, the molecular state data suggested for the violet azodiphosphonic acid derivatives an only four-center P–N=N–P chromophore with an electron-rich N=N center resulting from the different effective nuclear charges[7] N > P. To obtain additional quantum chemical information, our first π-type Hückel MO calculations were performed on the first IBM 3080 computer of the Max-Planck-Society in Munich using a Jacobi-type matrix diagonalization program[7]. In retrospect, the successful search for the origin of the azoviolet colour has taught us an unforgettable lesson on the rewards awaiting a preparative chemist investigating molecular states.

The three years from 1965 to 1968 were spent at the Federal Institute of Technology in Zürich under the guidance of Edgar Heilbronner to acquire some quantum-chemical experience, while coauthoring a three volume book on the "Hückel MO Model and its Application" (ref.[10]). During this time also the substituent effects of trimethylsilyl substituents on selected π-hydrocarbons were investigated by mass-spectroscopic determination of the first ionization energies, by polarographic measurement of the redox potentials and by UV/VIS spectra including those of suitable donor/acceptor complexes. The enormous electron-donating property of the β-silyl group was discovered[1b] and any silicon-d-orbital participation could be disproven[1b]. Other heteroelements such as boron or sulfur were also elucidated. In 1969, the move to the University of Frankfurt provided a chance to acquire several new instruments such as photoelectron (PES) and electron spin resonance (ESR) spectrometers and, above all, our first computer, a Hewlett–Packard 11/40. We learned how to properly assign radical cation state sequences[1,11] and radical dublet ground state ESR patterns[1,12] and also to approximate facets of molecular dynamics and reactions by hypersurface energy calculations[1,13]. Photoelectron spectroscopic ionization fingerprints were developed into an effective real-time gas analysis in flow systems[14].

The generation of interstellar molecules on Earth such as thioformaldehyde $H_2C{=}S$ and methylene imine $H_2C{=}NH$ or of unstable reaction intermediates such as diphosphorus P≡P, ethylidene ketene RHC=C=C=O or benzene silaisonitrile[14] $H_5C_6{-}N{\equiv}Si$, has provided information on the gas-phase fragmentation of molecules under unimolecular conditions ($p \approx 10^{-6}$ mbar). Real-time gas analysis in flow systems by photoelectron spectroscopic ionisation fingerprints[14a] including their assignment through highly correlated wavefunctions, which *vice versa* allowed us to identify the thermodynamically usually stable, but kinetically rather unstable species generated, proved to be of great advantage. Using the experience gained both experimentally[14] and from the accompanying hypersurface calculations[13], microscopic pathways could be tackled[15,16].

The first class of highly reactive and sometimes even explosive molecules selected was alkyl azides[15] such as the prototype methyl derivative $H_3C–N_3$ (Fig. 4) or even the tribosensitive vinyl azide $H_2C=CH–N_3$ which, once isolated as a solid, explodes on melting[15]. In contrast, when evaporated into a flow system under unimolecular conditions, there is no longer any danger. As discussed in detail (Chapter 3.1), pyrolysis pathways with elimination of the thermodynamically advantageous N_2 molecule as a driving force, partly precalculated and partly explained by hypersurface calculations, yielded a wealth of data including information on the dynamic behaviour observed in the chemical activation. Altogether the investigations[15,16], which might be characterized as an exercise in preparative physical chemistry (Fig. 4), illustrate what an inorganic or organic chemist can contribute to answering the still open question: "How do medium-sized molecules react?".

Another yet unanswered question, "What crystallizes how and why?" has stimulated efforts since 1989 to crystallize molecules and to determine their structure in the resulting molecular crystals, in which they are present usually in their ground state with largely "frozen" dynamics (Chapter 4.1). The static aspects of molecular self-assembly, therefore, can be considered to be a quite logical extension of previous studies on both molecular state properties (Fig. 3) and the microscopic reactions pathways of larger molecules (Fig. 4). In molecular crystals[17] (Fig. 5), the characteristic and often overlapping interactions lie in the following sequence of decreasing energy contribution: the solvation of cations, hydrogen-bridge bonding, donor/acceptor complex formation and van der Waals attractions. All of them can be of considerable importance in geo- or biochemistry, in solutions of molecular compounds or in the transition states of chemical reactions. The final target of this research project, however, is the self-assembly of molecules, for instance in lipophilically wrapped polyion aggregates (Chapter 4.2) such as $\{[(Ba^{\oplus\oplus})_6(Li^{\oplus})_3(O^{\ominus\ominus})_2]^{\oplus 11}\ (^{\ominus}OCR_3)_{11}(C_4H_8O)_3\}$ (Fig. 5), consisting of an elevenfold positively charged [octahedrane + prismane] cluster, which guarantees its thermodynamical stability and is covered by a hydrocarbon skin ($C_{56}H_{123}$), which provides both kinetic shielding and solubility in nonpolar solvents such as hexane.

The investigation of interactions in molecular crystals and, more recently, of self-organisation phenomena such as in lipophilically wrapped polyion aggregates (Fig. 5) is still in progress. The dynamics of crystallization and especially the generation of a crystal seedling are currently being studied intensely world-wide by numerous groups as indicated in the summarizing remark (Fig. 5): "Actually, everything is more complicated".

2. A USEFUL MOLECULAR STATE MODEL FOR THE PREPARATIVE CHEMIST

Our own efforts to measure and to explain molecular state properties, microscopic reaction pathways and the self-assembly of molecules (Chapter 1.2) should demonstrate what a preparative chemist, without any opportunity to study them *e.g.* by crossed beam

experiments analyzed by laser-spectroscopy, could contribute. An indispensible prerequisite for such a person in designing molecules and selecting appropriate measurement techniques to obtain the information desired, however, is a qualitative model to transparently rationalize the complexity of molecular states. The approach can be advantageously based on the results of instrumental analyses used day by day for investigations.

2.1. Molecular State Fingerprints in Instrumental Analysis

Of the numerous spectroscopic methods available for the characterization of compounds such as NMR, IR or UV/VIS, the more spezialized method of Ultraviolet Photoelectron Spectroscopy[1,4,11] has been chosen for an introduction, because of the information accessible in real time for isolated molecules in the gas phase and its transparent correlation with the results of quantum calculations via Koopmans' theorem, $IE_n^v = -\varepsilon_j^{SCF}$, or by highly correlated wave functions. For illustration, two examples will be presented, which are mainly of either academic (Fig. 6) or industrial interest (Fig. 7).

Numerous molecules have been detected by radio telescope screening of interstellar nebula[18a] such as Orion or Taurus M2; branched ones such as thioformaldehyde $H_2C{=}S$ are predominantly found in Orion[18a]. For its generation on Earth, methyl sulfur monochloride H_3CSCl has been chosen because, on heating under unimolecular condi-

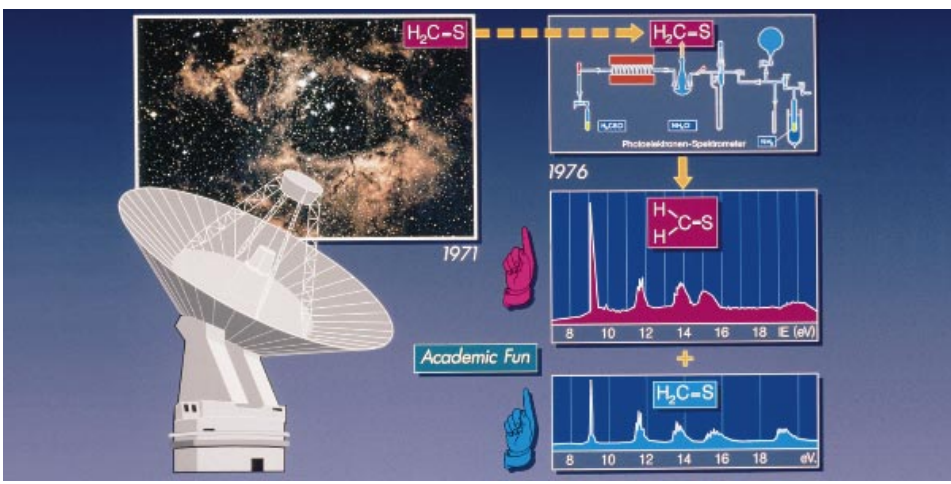

FIG. 6

Photoelectron spectroscopic radical cation state fingerprints for gas analysis in flow systems I: The generation of thioformaldehyde, detected by radiotelescope in interstellar space, on earth by pyrolysis, $H_3CSCl \rightarrow H_2C{=}S + HCl$, under stoichiometric addition of ammonia, $HCl + NH_3 \rightarrow [NH_4^{\oplus}Cl^{\ominus}]$, the ionization pattern recorded and its identification by calculation of a highly correlated wavefunction (*cf.* text)

tions ($p \approx 10^{-6}$ mbar), it selectively splits off HCl, which on stoichiometric injection of ammonia into the gas flow can be deposited as an nonvolatile salt [$NH_4^{\oplus}Cl^{\ominus}$] on the walls of a reaction bulb[14] (Fig. 6, upper right). The gas stream resulting after optimization of all the reaction parameters under continous recording of photoelectron spectra contains only $H_2C{=}S$ as proven by its ionization pattern, assigned by a highly correlated PNO-CEPA calculation (Fig. 6, lower right). This unequivocal identification of the thermodynamically stable, but according to the polymerization observed on attempted isolation, kinetically unstable $H_2C{=}S$, answers the Shakespearean question "To measure or to calculate?" by suggesting the combination of the two as being most advantageous[1a]. In contrast to generating an interstellar molecule on Earth, the detection of a molecule, first generated on Earth, in interstellar space by its known microwave spectrum has also been reported[18b]: Pyrolysis of the volatile pentacarbonyl chromium isonitrile complex, $(OC)_5Cr(NC{-}C(Cl){=}CHCl)$ under photoelectron spectroscopically optimized elimination of CO to non-volatile $CrCl_2$ yields the novel pentaatomic molecule acetylene isonitrile HC≡C–NC, which was later identified by its microwave spectrum to be present in the Taurus M2 nebula, containing predominantly linear molecules[18].

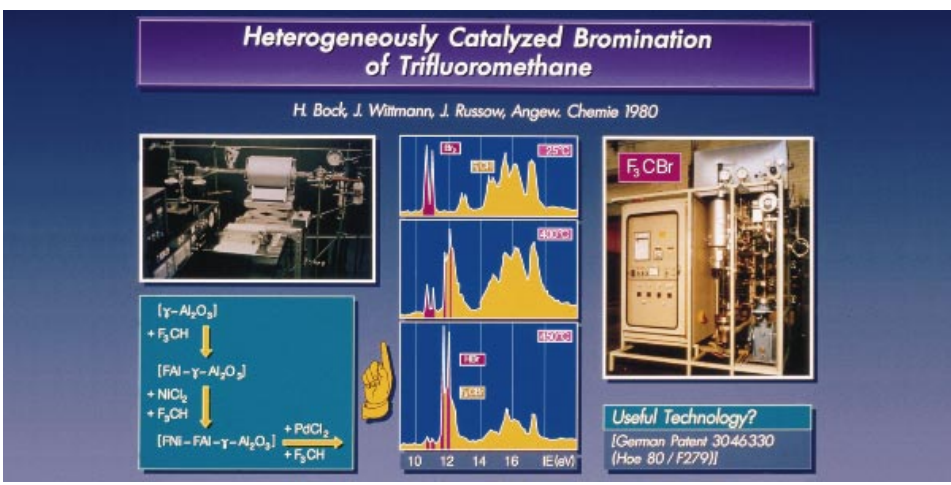

FIG. 7

Photoelectron spectroscopic radical cation state fingerprints for gas analysis in flow systems II: Development of a heterogeneous catalyst for the bromination of bromotrifluoromethane, $F_3CH + Br_2 \rightarrow F_3CBr + HBr$, to bromotrifluoromethane and optimization of the reaction conditions by diverting a fraction of the resulting reaction mixture via a pressure-reducing capillary into a spectrometer connected to the reaction tube outside the heating zone (*cf.* text) and the pilot plant constructed based on the PES results

The highly efficient real-time PES gas analysis, by which thermal reactions of millimole quantities of compounds can be scanned over a 1 000 degree temperature range within about six hours, also allows utilization of a change in the ionization fingerprints recorded for optimization of heterogeneously catalyzed reactions of industrial interest. One of the numerous published and/or patented projects concerns the development of a catalyst for the bromination of bromotrifluoroethane (Fig. 7).

Bromotrifluoromethane F_3CBr is a versatile industrial product, manufactured by bromination of trifluoromethane and well-known for its fire-extinguishing effectiveness. The thermal bromination at about 700 °C requires the handling of a highly corrosive mixture and, therefore, lowering of the temperature by a heterogeneous catalyst is of considerable advantage. To apply photoelectron spectroscopic gas analysis[14a] in both the catalyst and the reaction parameter optimization, a pressure-reducing (700 to 10^{-3} mbar) capillary had to be inserted into the reaction tube outside the heated reactor[14b] (Fig. 7, upper left). The only partly overlapping ionization fingerprints of the bromination mixture components and their change with increasing temperature (Fig. 7, center), especially the intensity decrease for Br_2 and the increase for HBr, permitted development of a highly selective and persistent catalyst within a few weeks (Fig. 7, lower left): γ-aluminium oxide was surface-fluorinated by heating in a F_3CH gas flow and both the Ni catalyst and the Pd promotor were each analogously fluorinated on top of the carrier. Based on the reaction parameter optimization by PES gas analysis, the bromination of trifluoromethane was further optimized in an industrial pilot plant (Fig. 3, right).

The three examples selected, $H_2C{=}S$ (Fig. 6), $HC{\equiv}C{-}NC$ (ref.[18b]) and F_3CBr (Fig. 7), as well as numerous additional ones[1,14], illustrate the intimate relationship between preparative chemistry and the molecular state approach needed for the instrumental analysis of reactions and their products. The advantage of combining the two approaches is obvious and poses the question of whether a more general and qualitative model can be recommended, which would simplify the complexity of the molecular state manifold by transparent principles and could help the chemist in the design of experiments by selecting suitable compounds and adequate measuring methods.

2.2. Molecular State Facets: Topology, Symmetry, Effective Nuclear Potentials as well as Electron Distribution and the Structure ↔ Energy Relation

Molecular states, as was pointed out in the introductory remarks (Chapter 1.1), enlarge the manifold of chemical compounds by also specifying their energy[1]. The individual states are grouped along their total energy scale (Fig. 8: A), starting from the ground state of the neutral molecule denoted $\Gamma(M)$ in the order of increasing energies *via* its nuclear spin and vibrational states (Fig. 8: NMR and IR) to the UV/VIS electronically excited ones denoted $\chi_i^j(M)$, each with vibrational sublevels. At higher energy, the molecule is ionized to the dublet ground state $\Gamma(M^{\bullet\oplus})$ of its radical cation, for which the spin distribution can be deduced from its ESR multiplet signals, as well as to elec-

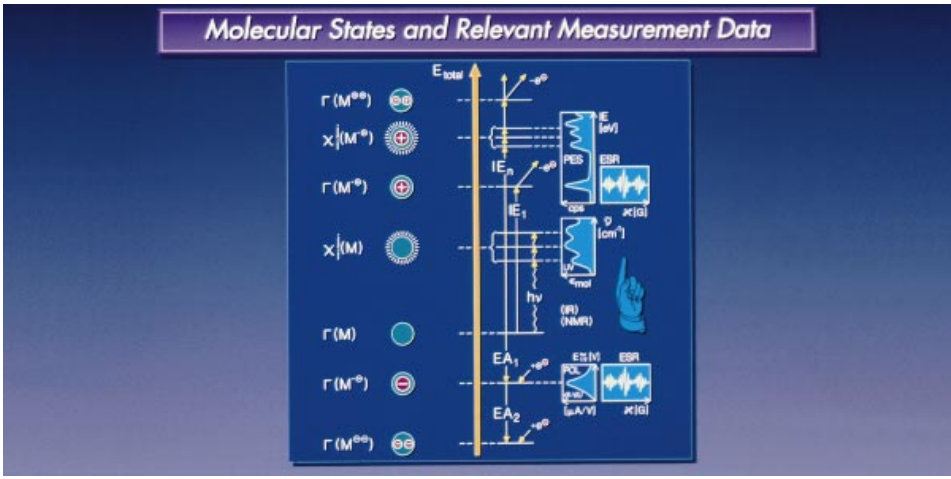

FIG. 8

Molecular state facets for the preparative chemist I: Schematic total energy scale for electronic ground (Γ) and excited (χ_i^j) states of a neutral molecule M and its radical cations $M^{\bullet\oplus}$ or dications $M^{\oplus\oplus}$ generated by ionization or oxidation and its radical anions $M^{\bullet\ominus}$ and dianions $M^{\ominus\ominus}$ resulting from electron insertion. In addition, the measuring methods used by the Frankfurt group are indicated, especially UV, PES, ESR, and ENDOR spectroscopy as well as polarography (POL) or cyclic voltammetry (CV).

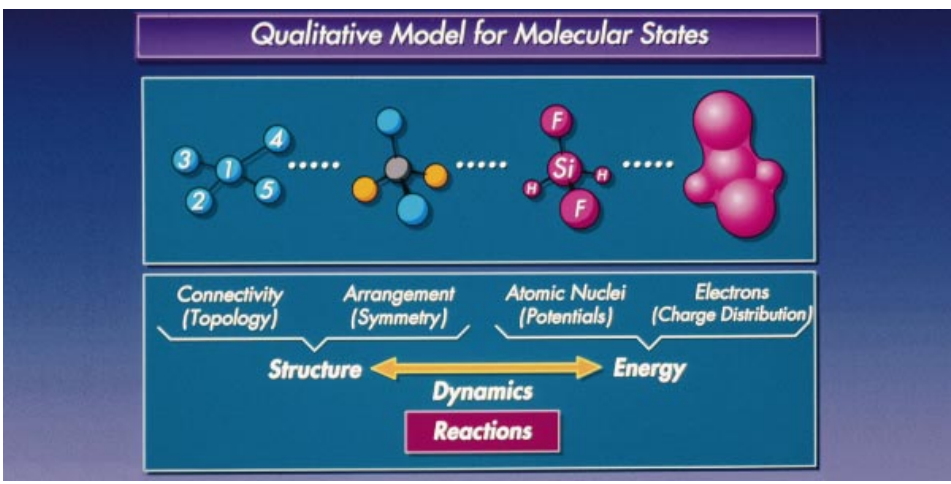

FIG. 9

Molecular state facets for the preparative chemist II: Qualitative model based on topology, symmetry, effective nuclear potentials and electron distribution and emphasizing the structure ↔ energy relation as well as molecular dynamics as an essential prerequisite in discussion especially of gas-phase reactions (*cf.* text)

tronically excited states as reflected in the PES ionization pattern. Still higher energies or oxidation in a stabilizing solvent can generate a dication by expelling another electron, and so forth. On the negative total energy side relative to the ground state Γ(M) lie the molecular radical anions and polyanions such as the rubrene tetraanion, generated in aprotic THF solution by reduction at a sodium metal mirror and structurally characterized as a solvent-shared contact ion quintuplet[19] $[(H_5C_6)_4H_8C_{18}^{\ominus\ominus\ominus\ominus}(Na^{\oplus}THF_2)_4]$.

In the explanation of individual molecular states and of their properties measured (Fig. 8) or calculated by highly correlated wavefunctions (Fig. 6) and their comparison, essential for the preparative chemist in series of chemically related or even iso(valence)electronic compounds (Fig. 3), a simplifying qualitative model proved to be quite useful[1] (Fig. 8). Two of its components, the topological connection of the centres within a molecule and their spatial arrangement as denoted by symmetry, represent the molecular structure. The other two components are the effective nuclear potentials within the molecular skeleton and the resulting electron distribution, which permit approximation of the relative energy of the respective molecular state. Together, they establish the fundamental relation between the structure and energy of molecules: Energy differences, which affect the given electron distribution within a molecule will change its structure. To cite just a few of the numerous molecular distortions observed in spectroscopic studies[1]: on $\pi\rightarrow\pi^*$ excitation of ethylene, its molecular halves twist, linear acetylene bends and there are molecular states in which water becomes linear or carbon dioxide non-linear. One of the chemical consequences is that any oxidation or reduction of a compound *i.e.* removal or uptake of electrons, will necessarily change the product structure relative to that of the precursor.

The qualitative molecular state model (Fig. 9) is recommended for day-to-day use in the laboratory both in the design of experiments and in discussion of their results, because it can be easily parametrized and/or calibrated by available measured data ranging from structural parameters *via* spectroscopic or electrochemical energy differences to known substituent perturbation effects[1]. In addition, it can be supported by quantum chemical calculations ranging from semiempirical *via ab initio* and density functional to correlated ones. All of them advantageously start from structural data, depending on the approximation chosen, provide valuable information on total energies of various molecular states (Fig. 6) or their charge distribution. In particular, the results calculated for a specific variation of the molecular topology, symmetry or potentials (Fig. 9) reveal the electronic and/or the dynamic flexibility of the ensemble studied. Hypersurface calculations for selected molecular degrees of freedom assist in understanding perturbation effects and provide some insight into certain aspects of molecular dynamics[1,13]. To further illustrate the applicability of the qualitative molecular state model (Fig. 9) and to demonstrate its usefulness, the following examples are selected to portray the individual facets.

Topology (Fig. 10): The about 10^7 compounds registered in Chemical Abstracts are stored in its Database in terms of incidence matrices specifying all bonds through con-

nectivities between individual centres. For the ensemble C_6H_6 selected and for carbon coordination numbers up to four, altogether 217 potential topological isomers are predicted, which include known molecules such as cyclic benzene or linear diacetylene as well as numerous unknown ones. Because their structures can be optimized quantum chemically and enthalpies of formation calculated[20a], the advantage of a preliminary computer screening for potential products of a novel reaction is obvious. In addition, the topology of molecules leads to specific eigenvalue patterns for *e.g.* cyclic or linear systems[1a], which can be parametrized by molecular state measurement data *e.g.* for polysilanes[20b,c], and thus permit comparison of known compounds and even predictions for unknowns ones[1]. Furthermore, topological definitions such as the more general one of alternancy can be very helpful in understanding otherwise unexpected experimental results such as the identical ESR spectra measured for radical cations and radical anions of alternating π-hydrocarbons[1a,20d]. Summarizing, molecular topology is an appropriate facet of a qualitative molecular state model for the chemist.

Symmetry (Fig. 11): Topological graphs for chemical compounds are by definition only two-dimensional and, therefore, the characterization of the spatial arrangement in three-dimensional molecules also requires knowledge of its symmetry. In close analogy to topology, it also represents a rather general quantity with numerous additional applications for molecules, ranging from the varying overall symmetry during structural changes to the notation of vibrational modes or of radical cation states by irreducible representations. For a transparent example, the thermal decarbonylation of 3,4-bis(methylthio)cyclobutene-1,2-dione to bis(thiomethyl)acetylene is chosen[21a], which has been optimized by PES gas analysis (*cf.* Figs 6 and 7). Two preferred conformations are conceivable, a C_{2h}-symmetric one with coplanar CS bonds or one of C_2 symmetry, in which they are perpendicular to each other. A one-dimensional energy hypersurface as a function of the torsion angle ω(CS–C=C–SC) predicts the (nearly) C_2 conformer with an 86° torsion angle to be thermodynamically more stable, a quantum-chemical result that can be confirmed by correlation of the angle-dependent eigenvalue pattern with the ionisation energies of the pairwise almost degenerate six lowest radical cation states measured PE spectroscopically[21a] and also by an independent electron diffraction determination of the molecular structure in the gas phase[21b].

Effective nuclear potentials (Fig. 12): In substituent π perturbation effects, those of first order[10] are largely determined by the effective nuclear potentials of the adjacent centers[1]. Within the Slater concept, they can be approximated by the atomic ionisation potentials, $Z_{eff} = (\overline{IE}_n\, n^2/\, 13.6)^{1/2}$, of the electrons of principal quantum number n and provide useful shielding constants, $A = (Z - Z_{eff})$, of the respective nuclear charge Z by electrons below and within the valence shell. The often tremendous changes in molecular state properties due to the differences in the effective nuclear charges are convincingly demonstrated by comparing the photoelectron spectra of the six-atomic molecules ethane and disilane[1b,11d], which each contain the C or Si centers connected to each other (Fig. 12): Both ionisa-

FIG. 10

Topology as an essential facet of a qualitative molecular state model for chemists is exemplified by the computer-predicted 217 isomers of the ensemble C_6H_6 for carbon coordination numbers up to four, which comprise well-known molecules such as cyclic benzene or linear diacetylene as well as numerous ones that are either unknown or could only be synthesized with stabilizing substituents (*cf.* text for other applications of topology)

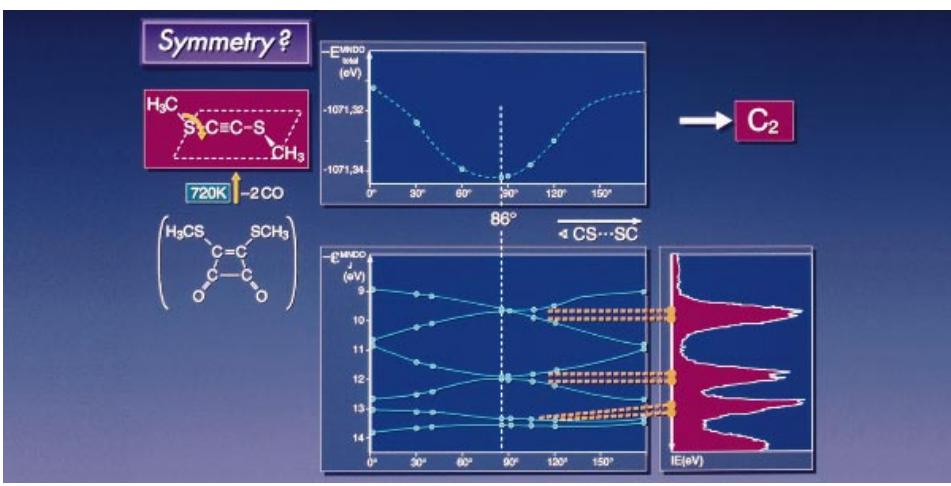

FIG. 11

Symmetry as an essential facet of a qualitative molecular state model for chemists is illustrated by the thermal decarbonylation of bis(thiomethyl)cyclobutene-1,2-dione to bis(thiomethyl)acetylene, the C_2-symmetric conformation of which is predicted by a one-dimensional energy hypersurface calculation for varying torsion angle ω(CS–C≡C–SC) and confirmed by correlation of the angle-dependent eigenvalue pattern with the PE-spectroscopic ionisation energies for the six lowest and pairwise almost degenerate radical cation states (*cf.* text for a more general application of symmetry)

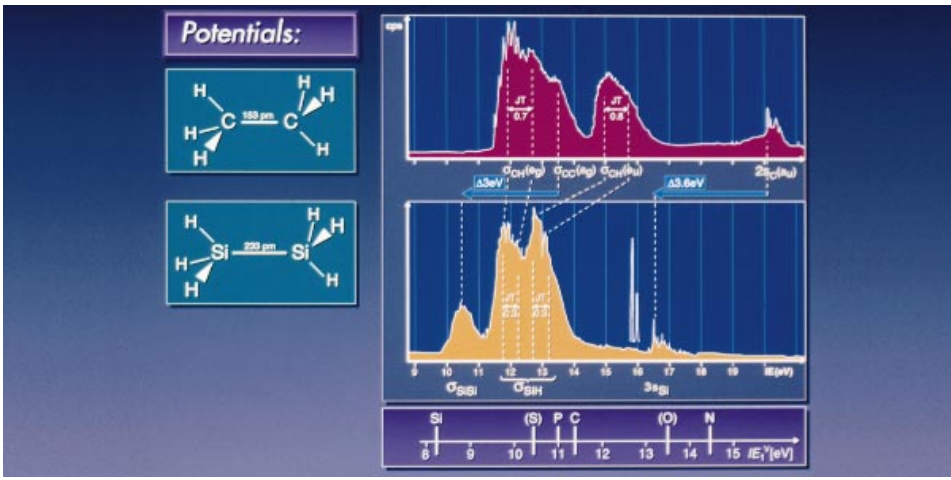

FIG. 12

Effective nuclear potentials as an essential facet of a qualitative molecular state model for chemists are demonstrated by the tremendous ionisation energy decrease of the radical cation states with dominant σ_{SiSi} and $2s_{Si}$ contributions in the photoelectron spectra of the iso(valence)electronic molecules ethane and disilane, which further confirm the sequence of Slater-type Z_{eff} values deduced from the ionisation potentials of the respective atoms (*cf.* text)

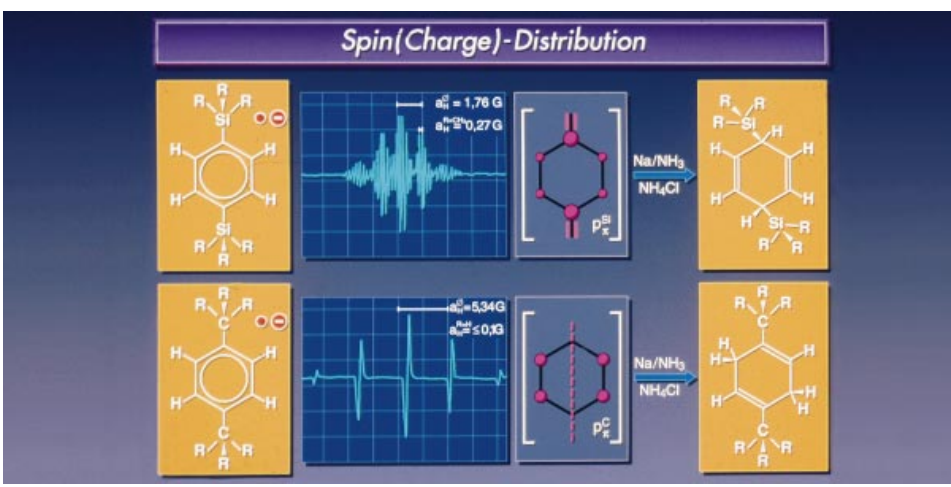

FIG. 13

Electron distribution as an essential facet of a qualitative molecular state model for chemists is visualized by the different Birch reduction protonation products of the iso(valence)electronic 1,4-bis(trimethylsilyl)- or 1,4-bis(*t*-butyl)benzene derivatives: ESR spectra of their radical anions demonstrate the presence of differing spin distributions with a nodal plane only in the $(R_3C)_2$ substituent axis and, assuming an analogous charge distribution in the dianions generated by Birch reduction, their $NH_4^{\oplus}X^{\ominus}$ quenching expectedly yields either only cyclohexadiene-2,5- or only -1,4-derivatives (*cf.* text)

tion energies to the radical cation states $(H_3X–XH_3)^{\bullet\oplus}$ with dominant contributions σ_{XX} or ns_X are drastically lowered by 3.0 eV or 3.6 eV (!), respectively. The shift of the σ_{SiSi} PES band out of the σ_{SiH} ionisation hill to $IE_1^v = 10.5$ eV, separated by more than 1.5 eV from the next radical cation state and indicating why doped polysilanes are electric conductors[11e], is specially remarkable. There are numerous other consequences of the rather low effective nuclear charge of Si centers, such as the powerful electron donor effect of β-trimethylsilyl groups, which allows adequately substituted π-hydrocarbons to be oxidized in $AlCl_3/H_2CCl_2$ solution to their radical cations[1b,11d,12].

Electron distribution (Fig. 13): Obviously, the electron distribution in a molecule over the effective nuclear potentials in its framework must be an essential facet of a qualitative molecular state model for chemists (Fig. 9). From the uncountable relevant examples, the reduction of 1,4-di(*t*-butyl)- and 1,4-bis(trimethylsilyl)benzenes to their radical anions and dianions is chosen, because it demonstrates the day-to-day usefulness of the model in laboratory work. To begin with, the ESR spectrum of the trimethylsilyl substituted radical anion exhibits a quintet for the four phenyl hydrogens, further split by the 18 methyl hydrogens. In contrast, the *t*-butyl substituted species exhibits larger coupling, but no additional multiplet splitting, which suggests a spin nodal plane along the substituent axis and higher spin density at the unsubstituted phenyl carbon centres. Based on the often, but not always[22] justified assumption of a spin-like charge distribution even in the molecular dianion, a Birch reduction with sodium in liquid ammonia has been performed and the reaction mixture quenched by adding ammonium chloride. The expected protonation at different phenyl carbon centers is indeed observed: the silylated dianion yields exclusively the corresponding cyclohexadiene-2,5 derivative, whereas only the cyclohexadiene-1,4 product is isolated from the alkylated dianion.

Examples have been selected to illustrate useful applications of the qualitative molecular state model for chemists (Fig. 9): for *topology* the prediction of the 217 isomers in the ensemble C_6H_6 (Fig. 10), for *symmetry* the gas phase structure of $H_3CS–C{\equiv}C–SCH_3$ predicted by hypersurface calculation and confirmed by its ionisation fingerprint (Fig. 11), for *effective molecular potentials* the tremendous differences in ionisation energies observed for the iso(valence)electronic molecules $H_3C–CH_3$ and $H_3Si–SiH_3$ (Fig. 12), and for *electron distribution* both the different ESR spectra of iso(valence)electronic, R_3C and R_3Si substituted benzene radical anions as well as the different structures of their Birch reduction products (Fig. 13). All of them demonstrate convincingly the prediction and explanation of various molecular state properties.

2.3. Time-Scale and Molecular Dynamics

Molecular state phenomena and their measurement are often classified as being either vertical or adiabatic with a border-line of about 10^{-14} s between the two: Vertical processes occur in time intervals of about 10^{-15} s or shorter and consist exclusively of electron movements such as excitation or ionisation of molecules as well as the accompanying changes in the

charge distribution. In contrast, adiabatic processes are observed at about 10^{-14} s or longer time intervals and are characterized by the onset of vibrational molecular dynamics, which causes changes in the molecular structure and allows relaxation or dissociation in molecular states of excessive energy. The schematic time scale for molecular states and their changes (Fig. 14), shows for microwave or radiowave excited molecules that molecular rotations as well as spin resonance phenomena can be observed and, for instance, proton or electron transfer, followed at larger time intervals by chemical transformations.

Reviewing the molecular state properties already discussed (Chapters 1.2, 2.1 and 2.2), time scale and molecular dynamics play an important rôle: To begin with the vertical ionisation of molecules to their various radical cation states in the femtosecond range (Fig. 14), fast electron expulsion leaves the radical cation with a "frozen" structure of the neutral molecule. Because of the absence of structural changes, photoelectron spectra often can be assigned through the eigenvalues ε_J^{SCF} of uncorrelated quantum chemical calculations *via* Koopmans' theorem, $IE_n^v = -\varepsilon_J^{SCF}$. In contrast, ESR spectra recorded in solution on microwave irradiation, exhibit molecular dynamics at least at higher temperatures, when the rigid matrix becomes a liquid and the necessary activitation energies can be supplied.

Under adiabatic conditions, numerous and temperature-dependent molecular dynamics phenomena in molecular radicals and radical ions have been observed. An especially lucid example is the dithiolane radical cation[23] $(S_2(CH_2)_3)^{\bullet\oplus}$: It contains a five-membered ring with two connected sulfur centers, whose pseudoration and its activation can be observed in ESR experiments at various temperatures (Fig. 15) and, in addition, can be simulated by a quantum chemical hypersurface calculation (Fig. 16).

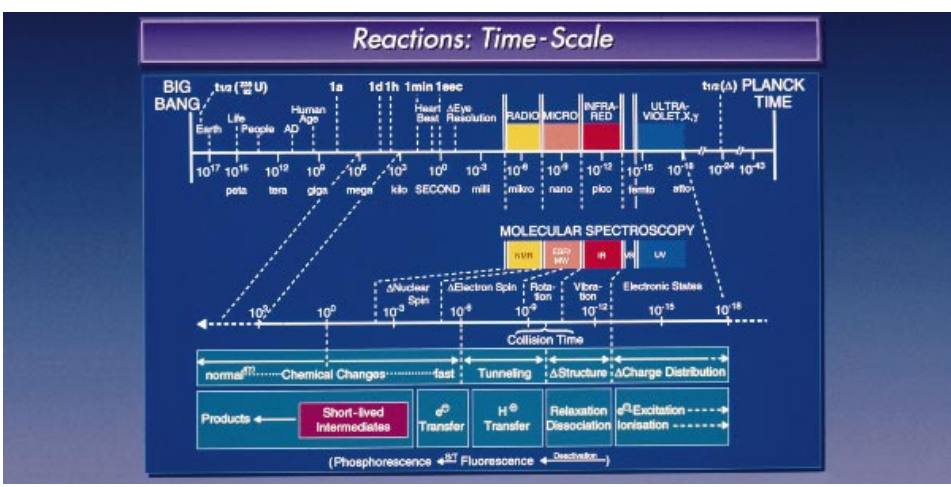

FIG. 14

Schematic time-scale for molecular states and their changes (in seconds, the approximate time interval between human heart beats as well as the resolution of stimuli by the eye)

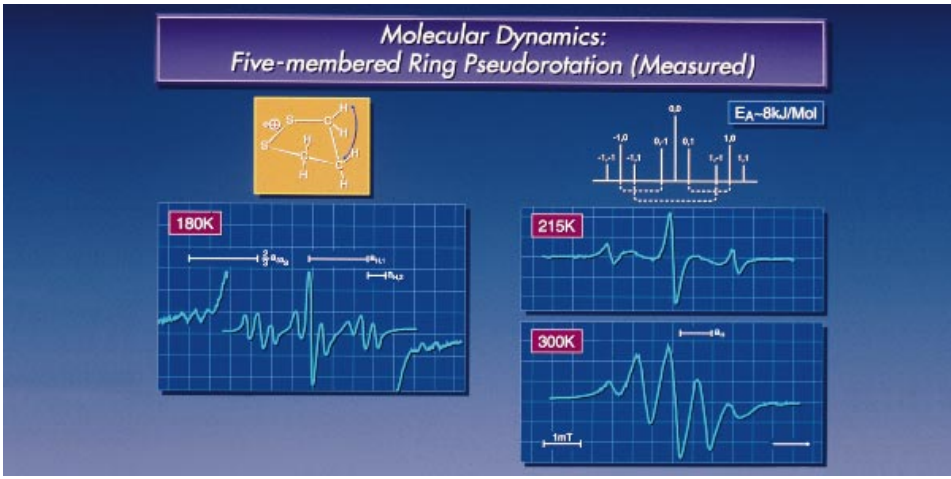

FIG. 15

1,2-Dithiolane Radical Cation: (A) Generated by oxidation with $AlCl_3$ in H_2CCl_2 solution at 180 K, the two different hydrogens of the two H_2C groups flanking the $SS^{\bullet\oplus}$ center each gives rise to an ESR signal pattern consisting of a triplet of triplets, which changes as a result of activation of the ring pseudorotation above 200 K to a quintet for the dynamically equivalent four hydrogens at 300 K

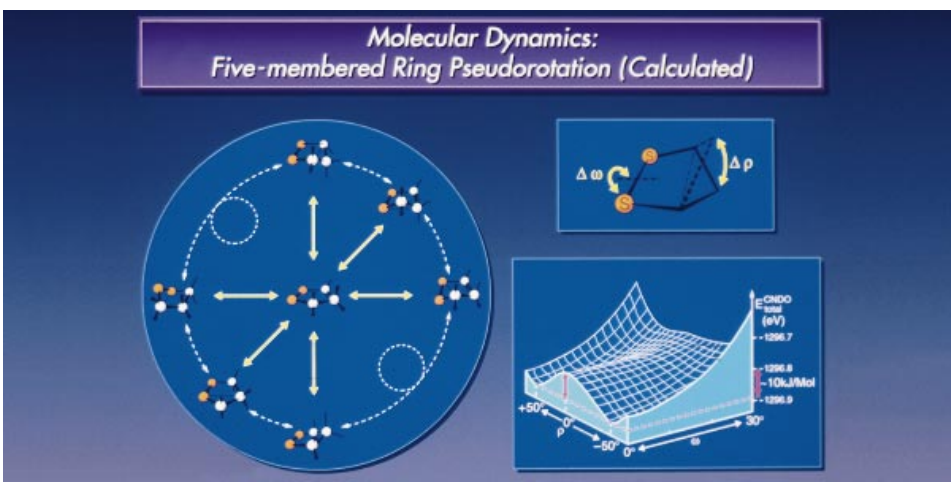

FIG. 16

The dithiolane pseudorotation depicted schematically and an approximate CNDO hypersurface which has been calculated by overlapping the two dominant vibrational modes of ring twisting and bending in the $N = 11$ center molecule with altogether $3N - 6 = 26$ degrees of freedom (*cf.* text)

Pseudorotation of five- and six-membered rings is a fascinating and thoroughly studied molecular dynamics phenomenon of considerable complexity. The simplified scheme depicted (Fig. 16, left) is based on the topological enumeration (*cf.* Fig. 10) of six different conformers[23], which can be transformed into each other either by rotation within the ring (Fig. 16, left, periphery) or by swinging the respective ring center through a planar intermediate (Fig. 16, left, center). This rather drastic simplification of the altogether $3N - 6 = 27$ degrees of freedom for the $N = 11$ centre molecule 1,2-dithiolane, however, permits calculation of the total energy hypersurface (Fig. 16, bottom right), which exhibits two minimum valleys for out-of-plane bending angles $\varphi = \pm 50°$, in which the molecule "swings" with variation of the torsion angle ω. The activation barrier calculated for both dynamic modes of each about 10 kJ mol^{-1} almost coincides with the experimental value of about 8 kJ mol^{-1} for the radical cation, determined from Arrhenius plots $\ln k/(1/T)$ of the temperature-dependent ESR signal pattern[23] (Fig. 15).

There are several lessons to be learned here: Molecular dynamics makes an essential contribution to molecular state phenomena investigated under adiabatic conditions. Its complexity especially in larger molecules with many degrees of freedom can only be approximated for certain geometrical situations. Topological conformer enumeration[23] or symmetry analysis of dominant vibrational modes are helpful to specify possible reductions in the number of degrees of freedom. As discussed below in detail for the thermal fragmentation of methyl azide under unimolecular conditions (Chapter 3.1), molecular dynamics, above all, play an essential rôle in chemical reactions.

3. MICROSCOPIC REACTION PATHWAYS OF MEDIUM-SIZE MOLECULES

In the introductory remarks (Chapter 1.1) it was emphasized that molecular states of specific energy (Fig. 8) are the real building blocks of the chemist. Therefore and as exemplified by photochemistry, the reactivity of molecules will usually differ with their energy-dependent electron distribution, which also changes the potential framework structure (Fig. 9). In addition and especially for larger molecules with N centres and $3N - 6$ degrees of freedom, molecular dynamics (Chapter 2.3) may be important, as is obvious for thermal fragmentations in the gas phase.

Microscopic reaction pathways of smaller molecules have been intensely investigated over many years (*cf. e.g.* the Nobel Prize 1986: D. R. Herschbach, Y. T. Lee and J. C. Polanyi) and, using femtosecond laser spectroscopy, transition states have even been experimentally visualized[24]. For medium-size molecules, however, and in spite of impressive efforts in both measurements and quantum chemical calculations, the complexity of their microscopic pathways still provides a considerable challenge. Can the preparative chemist contribute at all to solving at least parts of the molecular reaction puzzle? Guided by facets of the qualitative molecular state approach (Figs 8 and 9), both the design of interesting precursor molecules and the optimization of reaction

conditions are feasible for future time-dependent studies using the measuring techniques of molecular physics.

In the following, examples are presented for the gas-phase fragmentation of reactive molecules under unimolecular conditions (Chapter 3.1) and for redox electron transfer in aprotic solutions accompanied by contact ion formation (Chapter 3.2). In these investigations either the vertical radical cation state fingerprints of photoelectron spectra (Chapter 2.1) or the adiabatically recorded ESR multiplet signal patterns (Fig. 13) have been used to trace facets of the respective microscopic reaction pathways.

3.1. Pyrolysis of Organic Azides under Unimolecular Conditions

Alkyl azides $RH_2C–N_3$ of medium size are ideal precursor molecules for thermal fragmentation studies in the gas phase[14]: In contrast to their tendency as liquids to violently explode when ignited in *e.g.* heavy metal-catalyzed decomposition, they can be heated in flowing systems under unimolecular conditions without danger[15]. The temperature-controlled elimination of N_2 as a thermodynamically advantageous leaving molecule, selectively generates alkyl nitrenes $\{RH_2C–N\}$ as both thermodynamically as well as kinetically unstable intermediates. Their rearrangements, which can be followed by adequate molecular fingerprints such as the PES ionisation patterns (Chapter 2.1) pro-

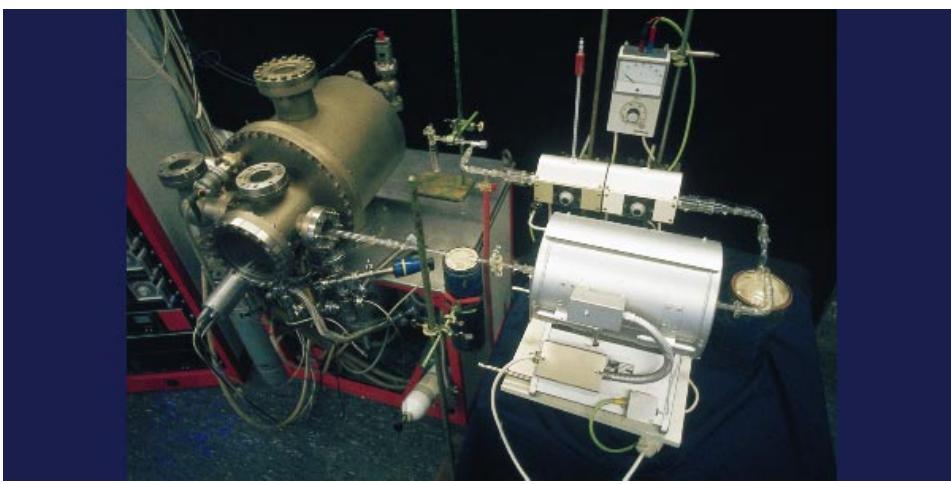

FIG. 17
Flow system apparatus for investigating the thermal fragmentation of molecules and their intermediates at various temperatures in the gas phase under unimolecular conditions starting at the precursor cooling trap, passing the first temperature-controlled reactor with a connected cooling trap for intermediate isolation; the second reactor is connected to the final product isolation trap and is attached to a photoelectron spectrometer, whose turbomolecular pump generates the flow

vide hints of a possible microscopic decomposition pathway[15]. An optimum apparatus for the studies (Fig. 17) consists of a cooling trap for the precursor molecule to adjust its vapor pressure, a temperature-controlled first oven zone for the N_2 split-off connected to a second cooling trap for liquid nitrogen condensation of intermediates and a second thermal reactor to initiate further fragmentation at higher temperatures, connected to a third cooling trap for final product isolation. The two reactor/three cooling trap-flow system is attached to a photoelectron spectrometer, whose turbomolecular pumps are used for evacuation and to generate the gas-flow. Above all, the continuously recorded PE spectra of the temperature-dependent gaseous product mixtures allow us to follow the individual reaction steps. The spectroscopic assignment and identification of the components can be readily accomplished by comparison with their preregistered PES band patterns or by calculating the unknown ones quantum chemically (Chapter 2.1).

Vinyl azide is an especially dangerous compound, because tribo-compression on melting the solid can trigger its violent explosion[15]. Because of the preparative effort needed to synthesize vinyl azide in millimole quantities and to handle it in a vacuum-line without freezing, elaborate quantum chemical precalculations have been performed in relation to potential expectations from its thermal fragmentation: For the ensemble

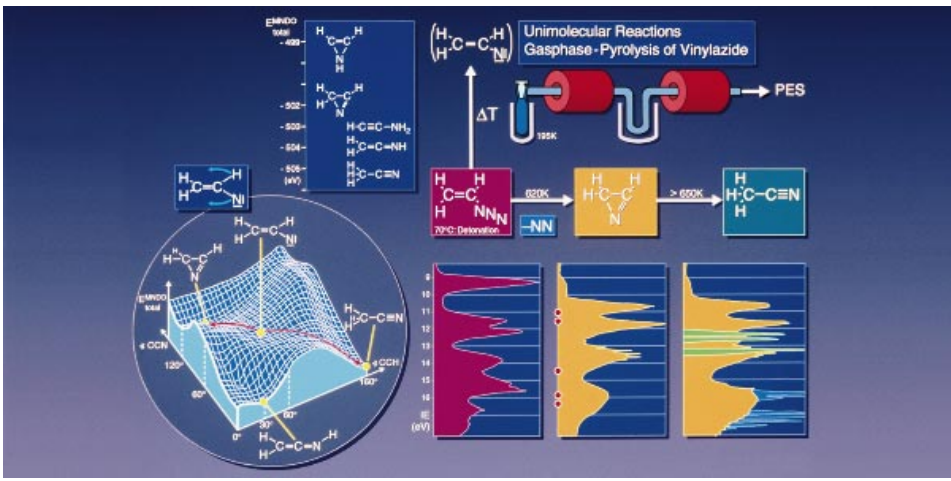

FIG. 18

The pyrolysis of vinyl azide in the gas phase under (nearly) unimolecular conditions (10^{-5} mbar) *via* N_2 split-off and consecutive, temperature-dependent rearrangements *via* 2*H*-azirine to acetonitrile: (a) Quantum-chemical precalculations both for the ensemble $\{H_3C_2N\}$ including vinyl nitrene and its potential isomerization products, partly projected onto a two-dimensional total energy hypersurface using angular coordinates (left-hand side). (b) Thermal N_2 split-off in a two oven-apparatus (Fig. 17) with 2*H*-azirine isolated in a cooled trap beyond the first heating zone and the products above 650 K, N_2 and H_3C–CN, characterized by their overlapping PE spectra (right-hand side; *cf.* text)

{H_3C_2N} resulting on N_2 split-off to the presumably unstable vinyl nitrene {H_2C=CH–N}, the topological isomers have been enumerated (*cf.* Fig. 10) and the total energies of their geometry-optimized structures have been semiempirically approximated (*cf.* Fig. 18, upper left). Accordingly, acetonitrile represents the global minimum, followed by ketenimine H_2C=C=NH < acetylene amine HC≡C–NH_2 < 1*H*-azirine H_2C(N)CH and – energetically rather improbable – 2*H*-azirine HC(NH)CH. A two-dimensional hypersurface, approximated by selecting out of the $3N - 6$ degrees of freedom the bonding angle, ∢HCC and the torsion angle ω(HC–CN), suggests a shallow local minimum for vinyl nitrene (Fig. 18, lower left) with a lower activation barrier to 2*H*-azirine and a higher one to acetonitrile. Rewardingly, all of the semiempirical predictions were fulfilled on synthesizing vinyl azide and decomposing it at various temperatures in the two oven/three cooling trap apparatus (Fig. 17): On heating to 620 K in the first reactor, the 2*H*-azirine could be trapped at about 100 K by cooling with liquid nitrogen and characterized by both its PES ionisation pattern recorded on re-evaporation and by its NMR spectrum[15]. On removing the cooling and heating to above 650 K in the second oven-zone, the continuously registered PE spectra exhibited both the ionisation bands of the N_2 leaving molecule as well as the known ones of the final thermal decomposition product, acetonitrile (Fig. 18, bottom right).

The thermal N_2-elimination from vinyl as well as other alkyl azides[15] is obviously a complex process which, even when the individual molecular dynamics (Chapter 2.3) are disregarded, raises numerous questions: Will short-lived nitrenes be formed initially and if so, in their excited singlet or in their triplet ground states? Do they rearrange rapidly to the imine derivatives, which can often be isolated (Fig. 18: 2*H*-azirine) or are the latter formed in an energetically favored synchronous process *via* ring closure (Fig. 18) or a 1,2-hydrogen shift (Fig. 19) coupled to the N_2-extrusion? Will imines always be intermediates in thermal alkyl azide fragmentations?

The gas-phase pyrolysis of the parent alkyl azide, $H_3C–N_3$, under unimolecular conditions provides additional information[15]. For vinyl azide (Fig. 18), two consecutive reaction channels are observed PE spectroscopically; in the first one N_2 is eliminated to form methanimine H_2C=NH, which also can be isolated (Fig. 4), and in the second one, H_2 is eliminated to form hydrogen cyanide HC≡N (Fig. 20, left, top equation). Extensive quantum chemical calculations have been performed for the N_2-extrusion, the overall results of which satisfactorily correlate with the experimental data[15]. To begin with, due to the large energy difference of about 600 kJ mol^{-1} between the triplet and singlet states, $X(^3A_2)$ and $A(^1E)$, of the nitrogen molecule expelled and because of the spin conversation principle, a singlet methyl nitrene $H_3C–N$ should be formed as the other pyrolysis product with an approximate activation energy of 220 kJ mol^{-1}. The second step in this asynchronous reaction sequence, the 1,2-hydrogen shift to methane imine, is calculated to be exothermic by about –400 kJ mol^{-1} (ref.[15]). In contrast, the synchronous reaction pathway of a 1,2-hydrogen shift coupled with N_2-extrusion should

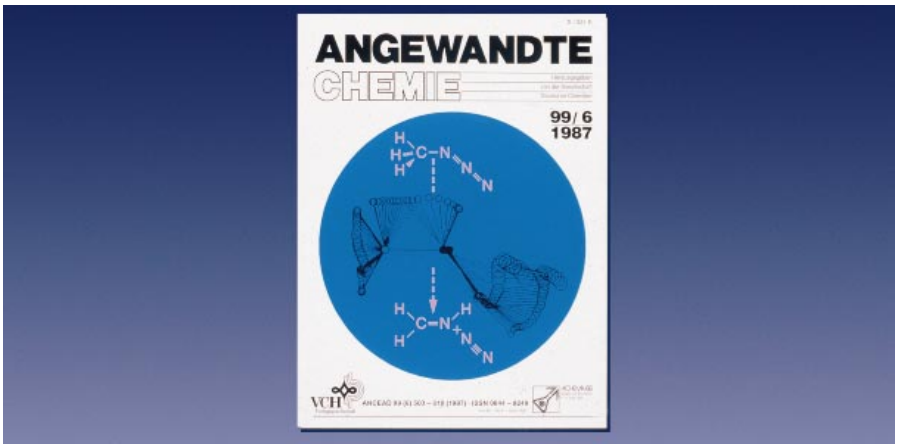

FIG. 19

Title page of Angewandte Chemie June 1987 presenting the semiempirically approximated reaction pathway for a synchronous N_2-elimination of methyl azide to yield methane imine: About 20 structures calculated along the total energy valley on passing over the saddle point are projected on top of each other, visualizing the change of the methyl (H_3C) to a methylene (H_2C) group, the hydrogen shift CH → NH and the shortening of the single bond C–N to a double bond C=N. Necessarily, however, the accompanying molecular dynamics is neglected (*cf.* text)

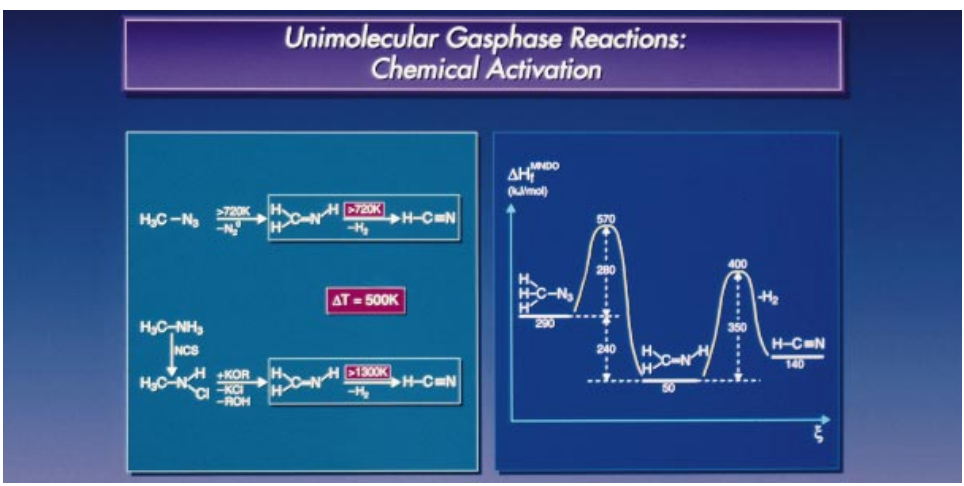

FIG. 20

Experimental evidence for the chemical activation of methane imine in its gas-phase generation from methyl azide by N_2-elimination: For the second consecutive reaction channel, $H_2C{=}NH \rightarrow HC{\equiv}N + H_2$, only a 50 K higher temperature of 770 K is needed. In contrast, if methane imine is prepared by dehydrochlorination of *N*-chloromethylamine, isolated and evaporated, then a 500 K higher temperature of 1 300 K must be employed for the dehydrogenation to hydrogen cyanide (left-hand side). The enthalpy diagram along the reaction coordinate for the consecutive N_2- and H_2-elimination from methyl azide (right-hand side) suggests that no additional activation energy is required for the second channel, in contrast to the H_2-elimination from re-evaporated methane imine, which needs to be fully activated

require an activation energy of only about 170 kJ mol^{-1}. It can be visualized by the stroboscopic projection on top of each other of about 20 structures (Fig. 19), calculated for moving the $H_3C–N_3$ molecule along its total energy valley and over the saddle-point of a three-membered ring. The 1,2-hydrogen shift from the H_3C substituent, transformed into a methylene H_2C group, to the nitrogen and the accompanying shortening of the single C–N bond to a double C=N bond are clearly recognizable; the extruded N_2 molecule leaves in a curved trajectory. Although the stroboscopically presented two-dimensional hypersurface calculation provides a rationale for a synchronous process $H_3C–N_3 \rightarrow H_2C=NH_2 + N_2$, it has to be pointed out, however, that the semiempirical approach (Fig. 19) necessarily neglects all molecular dynamics.

The important rôle of molecular dynamics is best demonstrated experimentally for the consecutive second reaction channel of the H_2-elimination from methane imine, $H_2C=NH \rightarrow H–C\equiv N + H_2$, to hydrogen cyanide (Fig. 20, left-hand side): If the methane imine is generated by methyl azide pyrolysis, this requires only a 50 K higher temperature of 770 K. In contrast, if $H_2C=NH$ is prepared by dehydrochlorination of *N*-chloromethylamine, isolated and re-evaporated, a 500 K higher temperature of 1 300 K (!) is needed to split off H_2 under comparable conditions in the very same flow system (Fig. 17). This surprising "chemical activation" of methane imine observed can be rationalized by its different origin: The excess energy stored in a molecule generated by a chemical reaction cannot be dissipated under unimolecular conditions in a gas stream due to the low collision frequency, whereas the isolated and re-evaporated compound requires the full activation energy to be supplied to enter the respective reaction channel. According to the enthalpy diagram along the reaction coordinate of the consecutive N_2- and H_2-eliminations from $H_3C–N_3$ via $H_2C=NH$ to $H–C\equiv N$ (Fig. 20, right-hand side), the methane imine formed in the first reaction channel should be "chemically activated" by approximately 340 kJ mol^{-1}.

The gas-phase pyrolysis of alkyl azides[15] as well as of other reactive molecules[14] – provided that the necessary precautions are taken! – proves to be not only a useful method for the preparation of otherwise not readily accessible compounds or an illustration of the advantagous PE-spectroscopic gas analysis, but in addition is particularly suitable for studying the still largely unknown microscopic reaction pathways of medium-size molecules with numerous degrees of freedom. And especially the proven formation of "chemically activated" intermediates should be of interest to other research groups with access to time-resolved measurement techniques.

3.2. Reduction of Quinones in Aprotic Solution

In exothermic reactions in solution, the reaction enthalpy stored as vibrational, rotational and translational energy of the resulting molecules is generally quickly dissipated by frequent collisions especially with solvent molecules. But in the network of equilibria, for instance, in redox reactions, which include electron transfer, ion solvation,

contact ion formation and aggregation[1d], other observations enables contributions to be made to the largely unknown microscopic reaction pathways of medium-size molecules. For a brief characterization of the numerous possible projects, classes of compounds, types of reactions, measurement techniques *etc*., the example of the reduction of 2,5-bis(trimethylsilyl)-*p*-benzoquinone without or with added lithium tetraphenylborate and studied by both cyclic voltammetry and ESR spectroscopy (Figs 8 and 13) is selected (Fig. 21).

The reduction of 2,5-bis(trimethylsilyl)-*p*-benzoquinone in aprotic DMF solution ($c_{H^{\oplus}}$ < 0.1 ppm) exhibits surprising changes on addition of the soluble salt $Li^{\oplus}[B^{\ominus}(C_6H_5)_4]$: Its second, reversible half-wave potential is lowered by 0.6 V (!) and simultaneously becomes irreversible[1d] (Fig. 21: CV). The presumed microscopic reduction pathway in the presence of excess lithium cation, which, owing to its small ionic radius ($r_{Li^{\oplus}}$ = 60 pm), possesses a high effective ionic charge $1/r_{Li^{\oplus}}$, is supported by independent ESR/ENDOR measurements[1d] in THF (Fig. 21: ESR): A 1 : 2 : 1 triplet is observed for the solvated radical anion $M^{\bullet\ominus}$, due to the two equivalent quinone hydrogens. The initially formed contact ion-pair radical $[M^{\bullet\ominus}Li^{\oplus}]^{\bullet}$ exhibits a decrease in symmetry from C_{2v} to C_s due to the "docking" of the $Li^{\oplus}$ ion and thus displays a doublet of doublets, the signals of which are each split into quartets by the ^7Li nuclear spin (I = 3/2). In the finally resulting triplet radical cation $[Li^{\oplus}M^{\bullet\ominus}Li^{\oplus}]^{\bullet\oplus}$, the quinone hydrogens are again equivalent and the two docked $Li^{\oplus}$ ions cause additional septet splitting. In this solvated contact triple ion, the final product, which will be the dilithium salt of 2,5-bis(trimethylsilyl)hydroquinone, is already preformed and, therefore, the second electron transfer takes place irreversibly at a dramatically lower reduction potential (Fig. 21: CV).

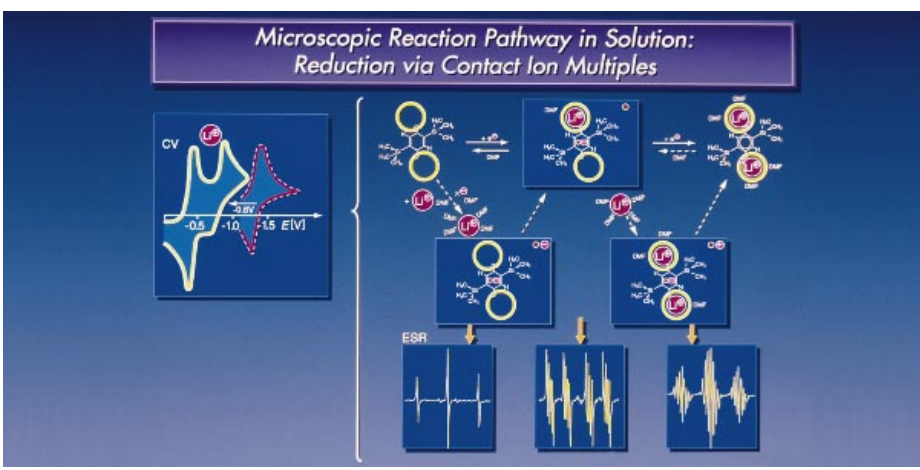

FIG. 21

Electron transfer and contact ion multiple formation on reduction of 2,5-bis(trimethylsilyl)-*p*-benzoquinone in aprotic solution by addition of $Li^{\oplus}[B^{\ominus}(C_6H_5)_4]$, discovered by cyclic voltammetry (CV) due to the tremendous decrease in the half-wave reduction potential and the contact ion multiples studied by the ESR multiplet signal patterns (*cf.* text)

The investigations have included other contact ion pairs of 2,5-bis(trimethylsilyl)-*p*-benzosemiquinone with larger and, therefore, more loosely coordinated counter cations[4], such as $K^{\oplus}$ ($r_{K^{\oplus}}$ = 138 pm). Additional approximate energy-hypersurface calculations[1d] surprisingly suggest that the $K^{\oplus}$ counter cation should "fluctuate": To reach the saddle-point 380 pm above the geometry-optimized six-membered ring of the quinone radical anion, an activation barrier of only approximately 30 kJ mol^{-1} would have to be surmounted. The predicted dynamics of the $K^{\oplus}$ contact ion pair can be confirmed by ESR spectroscopy (*cf.* Fig. 15): At 210 K, the expected doublet of doublets is measured for the nonequivalent quinone hydrogens, whereas at 295 K a ^1H triplet indicates that, owing to $K^{\oplus}$ fluctuation, the quinone protons become equivalent on the ESR time scale of 10^{-7} s (Fig. 14).

Altogether the CV and ESR/ENDOR data[1d], in combination with the quantum-chemical hypersurface calculations, as exemplified for 2,5-bis(trimethylsilyl)-*p*-benzoquinone, thus provide some insight into the pathway of a consecutive two-electron reduction, although solvent effects are still neglected. The partially dynamic contact ion pairs discovered in the investigation could be of interest both bioinorganically because of their carrier properties and industrially as molecular switches.

4. SELF-ASSEMBLY OF MOLECULES ON CRYSTALLIZATION

4.1. The Molecular State Approach to Molecular Structure

Radical cation ground-state characterization by ESR multiplet signal fingerprints (Fig. 8) also permits proof of the formation of radical ion pairs and multiples in aprotic solution by the metal counter-cation couplings observed[1d] (Fig. 21). ENDOR and especially ENDOR TRIPLE measurements, through which the electron/nuclear spin interactions and the signs of the coupling constants are accessible[5,25], reveal even finer details (Fig. 22, left-hand side): Complex ESR multiplet signal patterns such as recorded for the $Na^{\oplus}$ contact ion pair of 1-aminoanthraquinone radical anion are resolved into line pairs each centred around the usually well-separated Larmour frequencies of the respective nuclei. Additional TRIPLE experiments allow the different up-field and down-field line intensities to be employed to determine a positive sign for the ^{23}Na coupling and a negative one for the ^1H-coupling, suggesting that, as a consequence of necessary spin transfer *via* polarisation, the counter-cation must be located outside the π-nodal plane of the radical anion[26a]. For a general proof of this structural consequence deduced from the spin transfer mode as laid down in the frequently applied Hirota rules[5], the first radical ion pair ever has been crystallized and its structure determined[26b] (Fig. 22, right-hand side): From fluorene, selected for the large difference between its first and second reduction potentials, the radical anion was generated in aprotic DME solution under argon through contact with a sodium metal mirror promoted by ultrasonic sound and, on diffusing hexane into the solution for 20 h at –50 °C, red needles with a metallic

cluster crystallized. The structure determination in a cooled N_2 flow revealed the presence of a radical ion-pair dimer with two-fold DME-solvated, six-fold O-coordinated $Na^{\oplus}$ counter-cations[26b].

The successful crystallization of the first radical ion pair (Fig. 22), based on previous molecular state measurements and mastering all the experimental difficulties involved in the preparation and handling of an extremely air- and moisture-sensitive compound, opened a third research area for the Frankfurt group: After studying gas-phase reactions using ionisation fingerprints (Chapters 2.1 and 3.1) and after investigating radical ions including their dynamics and complex formation in solution using the ESR/ENDOR signal patterns (Chapters 2.3 and 3.2), the structure determination of interesting molecules and their molecular ions, designed according to the molecular state model described (Chapter 2.2), turned out to be a rather fascinating challenge[1d,17]. For such a project, the molecular state point of view proves to be especially advantageous for the chemist, because the structures of most molecules including spatially overcrowded ones as well as structural changes in their reactions can be predicted either from relevant measurement data (Figs 22 and 23) or by approximate energy hypersurface calculations (Fig. 24).

A transparent example for a measurement-predicted structure determination by electron diffraction in the gas phase is triisopropylamine, in which severe spatial over-

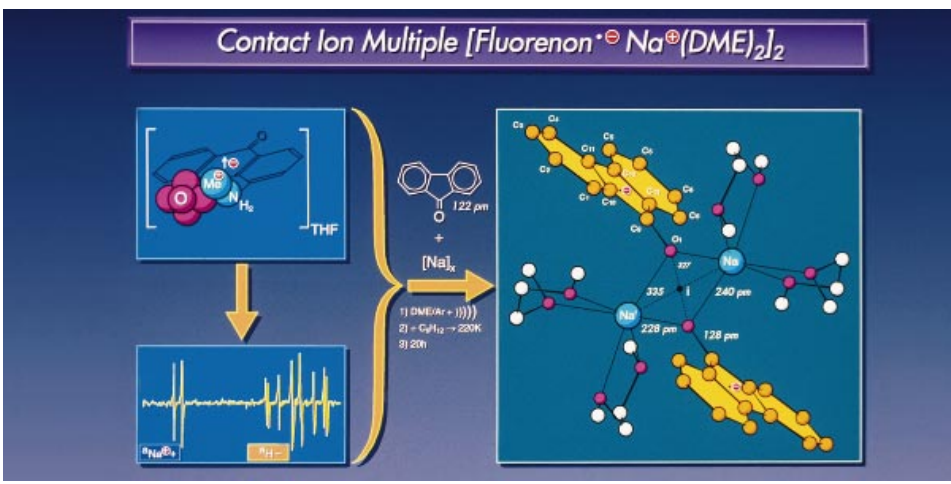

FIG. 22

Proof of contact ion-pair formation in solution by ENDOR and by crystallization: ENDOR TRIPLE spectrum of [$Na^{\oplus}$(1-aminoanthraquinone$^{\bullet\ominus}$)] in aprotic THF solution (left-hand side) and crystallization as well as structure determination of the radical ion pair [(fluorenone$^{\bullet\ominus}$)$Na^{\oplus}$(dimethoxyethane)$_2$]$_2$ (right-hand side), a dimer with six-fold coordinated $Na^{\oplus}$ counter-cations (*cf.* text)

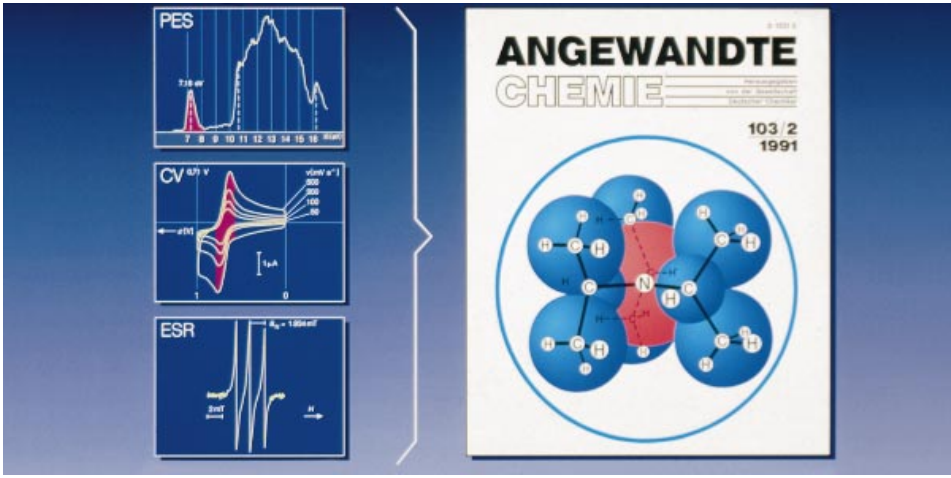

FIG. 23

Structure determination of triisopropylamine by electron diffraction in the gas phase confirmed a (nearly) planar C_3N skeleton as suggested by previous molecular state measurements comprising an extremely low first vertical ionisation potential (PES), a reversible first oxidation potential (CV) and an exclusively N-centred spin population (ESR), and the title page of Angewandte Chemie, February 1991 showing a graphic representation of the precalculated space-filling structure (*cf.* text)

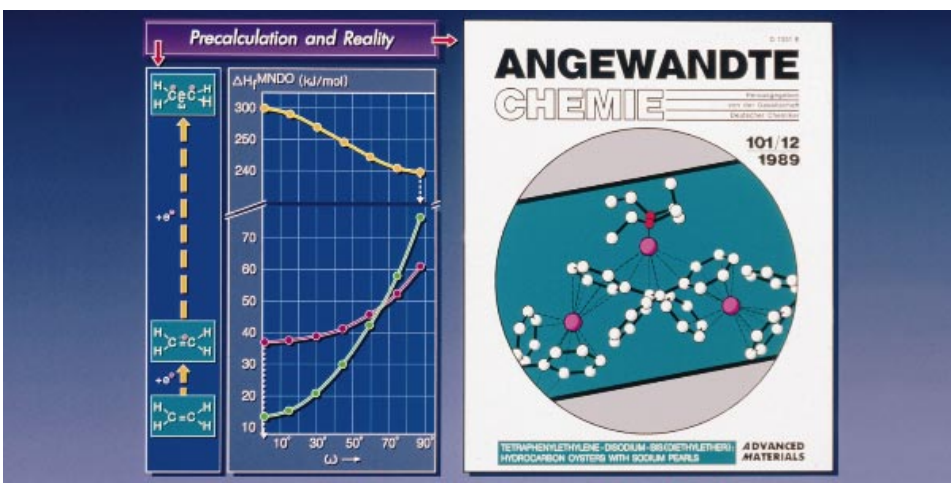

FIG. 24

Structure of the tetraphenylethylene dianion on the title page of Angewandte Chemie, December 1989 (right-hand side), crystallized as a polymer string of contact ion triples $[(H_5C_2)_2C^{\ominus}-{}^{\ominus}C(C_6H_5)_2(Na^{\oplus}(O(C_2H_5)_2)_2Na^{\oplus}]$ connected by benzene sodium sandwich links, and exhibiting molecular halves twisted relative to each other around the $C^{\ominus}-{}^{\ominus}C$ single bond and predicted by quantum-chemically calculated torsion potentials for ethylene, its radical anion and its dianion (left-hand side, *cf.* text)

crowding of its three bulky alkyl groups enforces a nearly planar C_3N skeleton with angles ∢ CNC of 119° (Fig. 23)[1d]. The compound can be prepared in a difficult three-step synthesis only in low yield, because the introduction of the third isopropyl substituent requires methylation by a solvent-free Grignard reaction at low temperature[27]. The molecule $((H_3C)_2CH)_3N$ exhibits an usually low first vertical ionisation potential of 7.18 eV (!), can be reversibly (!) oxidized at a cyclovoltammetrically determined potential of +0.71 V and the ESR spectrum of the resulting radical cation consists exclusively of a nitrogen 1 : 1 : 1 triplet with a_N = 1.934 mT and line widths of only 0.367 mT (Fig. 23)[27]. All the measurement data suggested a planar C_3N skeleton, which was further confirmed by additional MM2 force field as well as AM1-SCF calculations. The electron diffraction structure with the experimentally determined CNC angles of 119°, on the other hand, stimulated additional hypersurface calculations[27], which reproduced the expected shallow double minimum potential for the nitrogen inversion, reflecting another important facet of molecular dynamics (Chapter 2.3).

The structures of most molecules and especially of their molecular ion salts are preferentially determined by X-ray diffraction of single crystals, which contain the target species in the respective molecular ground state close to or even inside the global energy minimum and with largely "frozen" molecular dynamics. An analysis of crystal structures with negligible packing effects, therefore, provides an advantageous starting point for the discussion of numerous molecular properties and their quantum-chemical calculation. On the other hand, although the final crystal packing still cannot, in general, be anticipated[28], the charge perturbation in structures of molecular ions relative to the precursor molecules is readily accessible by SCF geometry optimization on various levels of sophistication. For instance, the initially surprising cyanine distortion of ethylene dianions or dications with their molecular halves twisted around the resulting $>C^{\ominus}–^{\ominus}C<$ or $>C^{\oplus}–^{\oplus}C<$ single bonds is predicted even by semiempirical torsion potentials (Fig. 24, left-hand side): The neutral $H_2C{=}CH_2$ within a steep potential well is D_{2h}-symmetric, while the shallower well for $H_2C^{\bullet\ominus}{-}CH_2$ agrees with experimental average twisting angles ω($R_2C–CR_2$) of about 20° for substituted ethylene radical anions[1d] and the unexpected prediction of an almost 90° angle for $H_2C^{\ominus}–^{\ominus}CH_2$ stimulated preparation, crystallization and structural analysis of the two-fold reduced tetraphenyl derivative (Fig. 24, right-hand side): Its $(H_5C_6)_2C^{\ominus}$ halves are found twisted by 56° around the 149 pm long single C–C central bond[29a]. The dianion is the essential subunit in the almost black polymer string of contact ion triples $[(H_5C_6)_2C^{\ominus}–^{\ominus}C(C_6H_5)_2(Na^{\oplus}(O(C_2H_5)_2)_2Na^{\oplus}]_{\infty}$, which are connected unexpectedly by intermolecular dibenzene sodium sandwich links. The tetrakis(dimethylamino)ethylene dication, prepared by chlorine oxidation, exhibits a twisting angle ω($N_2C^{\oplus}–^{\oplus}CN_2$) of 76° around a 152 pm long $C^{\oplus}–^{\oplus}C$ single bond[29b]. Both the dianion and the dication can be rationalized by cyanine distortion due to delocalization of the even number of four electrons over the odd number of three centers[1d].

Another example concerning an *intramolecular* dibenzene sodium sandwich in the contact ion pair of tetraphenylallyl anion, $[(H_5C_6)_2C–C(H)–C(C_6H_5)_2^{\ominus}Na^{\oplus}(O(C_2H_5)_2]$, prepared by reduction of tetraphenylallene with proton transfer from the solvent (Fig. 25, left), is presented in this introduction to the molecular state approach to molecular structure (Fig. 9). It is selected[1d], to further illustrate the well-established assumption that the calculated minimum of total energy represents the optimum charge distribution (Fig. 25, center and right-hand side): The analogous structure of the only diphenyl substituted model complex can be readily generated by MNDO geometry optimization using the Fletcher–Powell-subroutine programs (Fig. 25, center). Additional energy hypersurface calculations starting with the $Na^{\oplus}$ counter-cation close to one of the negatively charged 1,3-allyl anion centers results in its barrier-free movement into the center between the two phenyl rings which, according to an MNDO charge distribution analysis, is surrounded by ten ring-C-centers with a sum of –0.51 negative charges *i.e.* about 30% more than supplied by a single allyl anion-C-center. Even with cautious reservations concerning the parametrization of the semiempirical MNDO method, this unambiguous result from the enthalpy hypersurface approach supports the structure ↔ energy relation

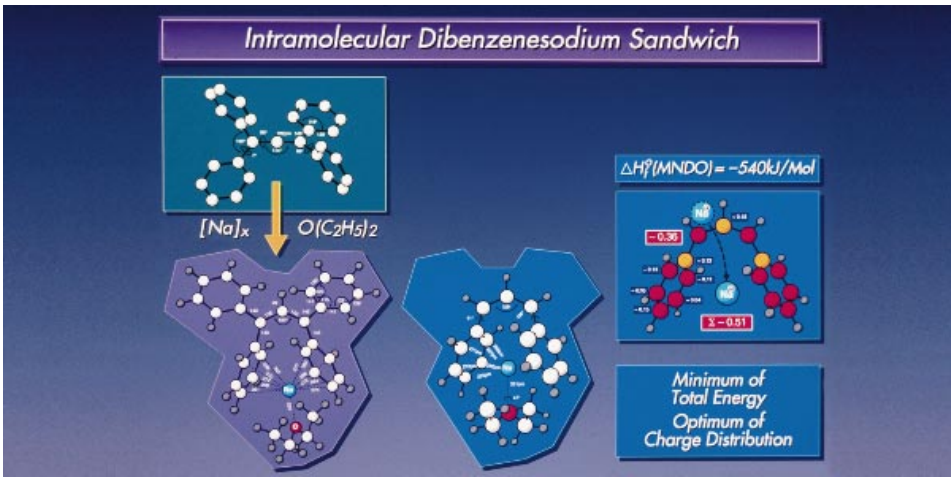

FIG. 25

Sodium metal mirror reduction of tetraphenylallene in diethyl ether solution and subsequent crystallization yields the contact ion-pair tetraphenyl anion–sodium–diethyl ether (right), for which the structure determination revealed an *intramolecular* dibenzene sodium sandwich, which also can be quantum-chemically calculated for the diphenyl substituted model compound (center). Additional enthalpy hypersurface calculations suggest that a $Na^{\oplus}$ counter-cation placed at one of the allyl anion centers moves barrier-free to a position between the two phenyl rings of highest surrounding negative charge (*cf.* text)

based on the charge distribution as do numerous other structures of contact ion multiples experimentally determined and rationalized by more elaborate density functional calculations[30].

The four examples from more than three hundred structure determinations by the Frankfurt group since 1990 have been chosen to demonstrate the advantageous molecular state approach for the design of interesting molecules and molecular ions guided by relevant measurement data (Figs 22 and 23) or by quantum-chemical calculations (Figs 24 and 25). In addition to the preparation of compounds, the "art of crystallization", which was the most widely used method to purify compounds in the last century and then partly abandoned, had to be acquired as did experience in structure determination under air- and moisture-free conditions at low temperatures. After two years of learning, a wider research project on interactions in molecular crystals could be started.

4.2. Interactions in Molecular Crystals

At the present time, the Cambridge Structural Database contains well over 10^6 individual structures of organic compounds ranging from medium-size ones to large polymers and including examples of unexpected molecular distortions, novel materials or biomolecular aggregates. Numerous books covering general as well as detailed aspects have been published[31] as have an ever increasing number of special feature reviews in various journals. The question posed, therefore, has been whether the molecular state point of view outlined for the design of new molecules or those of still unknown structure and based on measurement data or quantum-chemical calculations (Chapter 4.1) could continue to add valuable new facets. The Frankfurt group has embarked on studies of four, often dominant interactions in and between molecules (Fig. 26), which in the order of decreasing energy contributions involved might be termed cation solvation > hydrogen bridge bonding > donor/acceptor complex formation > van der Waals attraction and repulsion. Necessarily, the compounds had to be designed in such a way that no dominant interaction would obscure weaker ones that might be of interest in the respective study. Above all, methods had to be improved or developed to achieve – often with patience and tenacity – the crystallization of the molecular single crystals required and suitable for X-ray diffraction. With altogether 130 publications covering about 300 structures, obviously no complete overview can be accomplished within this context, but essential facts will be outlined emphasizing particularly the molecular state approach to the molecular structures proposed (Chapter 4.1).

Cation solvation: The thermodynamically favourable wrapping of cations by suitable solvent molecules is of essential importance for numerous processes from geology to biology, because the multi-dimensional equilibria networks *e.g.* of electron transfer, contact ion-pair formation and cluster aggregation are all decisively affected by solvation[1d]. Our studies[32] are represented by the contact ion triple $[perylene^{\ominus\ominus}(Na^{\oplus}DME)_2]$ in which the $Na^{\oplus}$ counter-cations are each μ^6-coordinated on the opposite side of the π-nodal plane.

When the number of oxygens is increased from 4 (two dimethoxyethane) to 5 (one tetraglyme), the $Na^{\oplus}$ is withdrawn from the perylene surface and becomes μ^1-coordinated at a single C center of its periphery and with 6 coordinating oxygens (one 18-crown-6) completely solvent-separated, leaving the then "naked" perylene dianion behind[32a]. To study the respective phenomena in more detail, $Na^{\oplus}$ counter-cations have been selected and their solvent-separated salts with large, well-delocalized π radical anions crystallized, which no longer form contact ion pairs. Based on the structural data, quasi-isodesmic calculations for the solvent complexes with and without $Na^{\oplus}$ have yielded enthalpies of solvation, which are valuable to the chemist in designing optimum conditions for solvent-dependent reactions[32b]. More recently, the structure of the first organic π-tetra-anion has been reported, crystallized as a contact ion quintuple[32a] [rubrene$^{\ominus\ominus\ominus\ominus}$$(Na^{\oplus}THF_2)_4$].

Hydrogen bridge bonding: In spite of well over 10 000 entries in the Cambridge Structural Data Base, numerous novel aspects of hydrogen bonding in single crystals of main-group element molecules are still being discovered world-wide. The studies of the Frankfurt group comprise both new preparative methods, aimed especially at hitherto unknown hydrogen-bridged molecular aggregates as well as double minimum potential calculations, predominantly to evaluate cooperative effects[33]. The first contribution

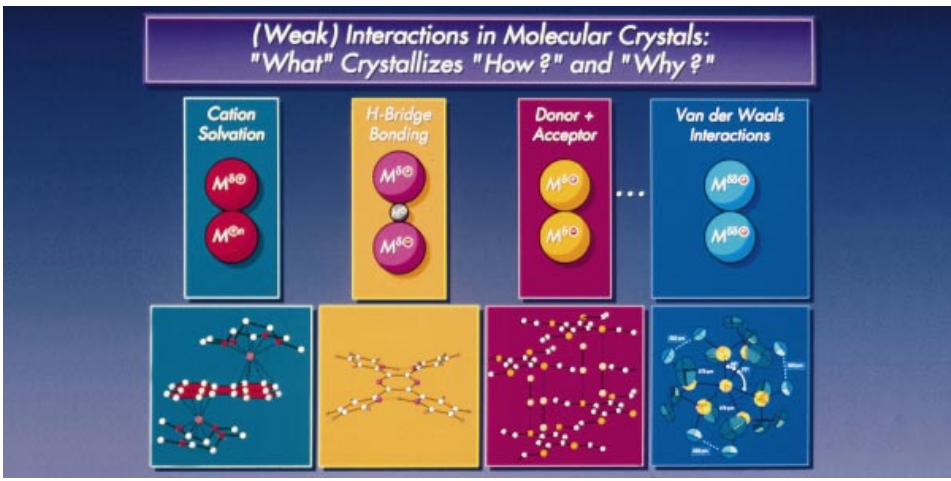

FIG. 26

Single crystal structure research program of the Frankfurt group in 1992–1996 aimed at specific interactions in molecular crystals such as (in order of decreasing energy contribution) cation solvation > hydrogen bridge bonding > donor/acceptor complex formation > van der Waals attractions and repulsions and represented (from left to right) by: the perylene dianion contact ion triple with DME-solvated sodium cations, the flattening of the tetrakis(2-pyridyl)pyrazine by intramolecular hydrogen bridges, the Br_2 adduct of 1,2,4,5-tetrakis(thioethyl)benzene or sterically overcrowded hexakis(trimethylsilyl)disilane (*cf.* text)

(Fig. 26, second structure from left) reported on the "chemical mimicry" (ability of animals to adjust in colour and/or shape to their environment) of the diprotonated tetra-(2-pyridine)pyrazine dication which, on replacement of the topotactive $Cl^{\ominus}$ $H^{\oplus}$-bridge acceptors in its di(hydrochloride) by non-protonable tetraphenylborate anions, is flattened by intramolecular short H-bridges and, therefore, turns dark yellow in colour[33a]. Nitro-substituted organic molecules provide new facets as expected from substituent perturbation (Fig. 9): For instance, diphenylnitromethane can be crystallized as an aci-nitro dimer containing a chair-like eight-membered ring with two OH…O bridges, for which an about 40% cooperative effect is quantum-chemically calculated[33b]. More recently, the shortest CH…O bridge found so far with a C…O distance of only 293 pm has been discovered in the double trinitromethane adduct to dioxane, $(O_2N)_3CH…O(CH_2CH_2)_2O…HC(NO_2)_3$, crystallized by careful purification of the explosive from dioxane solution[33c].

Donor/acceptor complexes: This most recent one of our research projects[34] started with single crystal growth of mixed-stack complexes, in which donor and acceptor components interact with each other in stoichiometric ratios. Based on the useful criteria of same skeletal symmetry and π overlap area, 21 complexes between π-donors such as alkyl or amino substitued benzene derivatives, pyrene or perylene with π-acceptors such as tetrahalogeno-*p*-benzoquinones or nitro/cyano substituted benzene derivatives have been crystallized[34a]. None of the structures determined for the deeply coloured compounds, however, showed any significant geometry change of the components due to π-stacking with interplanar distances of around 340 pm, *i.e.* the double π van der Waals radius of 170 pm and quantum-chemical calculations based on the crystal structure data did not reveal any donor → acceptor polarization effects at all in the ground state[34a]. Turning to smaller-size acceptors such as Br_2, with the fully substituent-perturbed, electron-rich donor 1,2,4,5-tetra(thioethyl)benzene black blocks crystallized, which surprisingly consist of tetrathiobenzene layers interconnected alternatingly by bromine sticks (Fig. 26, second structure from right). Relative to Br_2 molecules in the gas phase, the Br–Br distance is elongated from 227 to 240 pm, providing evidence for S → Br charge transfer from the sulfur donor centres[34b] which, according to density functional calculations, amounts to about –0.25 charges[30b]. In the meantime, for the redox disproportionation, $2\ I_2 \rightarrow I^{\oplus} + I_3^{\ominus}$, in the presence of a thiocarbonyl ligand $R_2C{=}S$, both the final product $[(R_2C{=}S)_2I^{\oplus}][I_3^{\ominus}]$ as well as the intermediate donor/acceptor complex $\{R_2C{=}S…I_2\}$ could be crystallized and their structures determined[34c].

Van der Waals interactions: Bulky tris(trimethylsilyl)silyl and tris(trimethylsilyl)-methyl substituents, $((H_3C)_3Si)_3Si–$ and $((H_3C)_3Si)_3C–$, are well-suited to design model compounds with spacers of different lengths between their half-shells, which permit study of *intramolecular* van der Waals interactions. In hexakis(trimethylsilyl)disilane (Fig. 26, structure at the right-hand side) due to steric crowding, the SiSi bond is elongated to 240 pm and the molecular skeleton $Si_3Si–SiSi_3$ of D_3 symmetry unexpectedly

exhibits two different dihedral angles of 43° and 77°, an appropriate criterion for steric crowding. In addition, C…C van der Waals distances of only 352 pm between some of the methyl groups are observed shortened by 12% relative to the sum of the van der Waals H_3C radii of about 200 pm, as a result of their cog-wheel meshing in the interior of the molecule[35a]. Extensive studies have dealt with the structures of polymorphic conformers of single molecules; this is already widely documented in the literature[31]. The Frankfurt group added several new facets such as monoclinic and triclinic modifications of tetraisopropyl-*p*-phenylenediamine, in which the nitrogen electron pairs are either perpendicular to the benzene ring plane with full n_N/π-delocalization or are coplanar, due to van der Waals repulsion between phenyl and isopropyl hydrogens[36b]. Crystal packing energy calculations predict the latter, monoclinic modification to be the more stable[36b]. For 2,2′-pyridylamine, in addition to the triclinic and orthorhombic modifications, a third monoclinic polymorph has been discovered[36c], and the phase transitions of the trimorphic system were analyzed by additional differential thermal analysis measurements[36c].

In summary, the preparation and crystallization of compounds and the structural characterization of numerous novel molecular single crystals by a team of highly motivated coworkers (Fig. 5) fully substantiated the usefulness of the molecular state model for chemists (Chapter 2.2). Structural analysis, complemented by quantum chemical and later by crystal packing energy calculations[36b] disclosed interesting details of inter-

FIG. 27

The single-crystal crystal structure of the barium–lithium–oxygen polyion aggregate $[Ba_6Li_3O_2]^{11\oplus}$ surrounded by eleven *t*-butanolate anions and three THF solvent molecules, which was crystallized from a THF solution and is the first example for the Frankfurt group of molecular self-organisation in lipophilically wrapped clusters (*cf.* text)

actions in or between molecules in solids and, together with the wealth of information accumulated in the Cambridge Structural Database, revealed multifaceted aspects for crystallisation as a phenomenon of molecular self-organisation[36].

4.3. Lipophilically Wrapped Polyion Aggregates

Our first lipophilically wrapped polyion aggregate, an (octahedrane + prismane) polyhedron $[(Ba^{\oplus\oplus})_6(Li^{\oplus})_3(O^{\ominus\ominus})_2]^{11\oplus}$ within an oxygen-containing hydrocarbon skin $\{C_{56}H_{133}O_{14}\}$ (Fig. 27), was discovered by serendipity: Barium metal was dissolved in *t*-butanol with butyllithium added to react with the water expected from *t*-butanol dehydration and the resulting precipitate was dissolved in THF, from which colourless prisms crystallized. Relativistic density functional calculations demonstrated the presence of an ionic cluster core with $O^{\ominus\ominus}$ dianions both in the $(Ba^{\oplus\oplus})_6$ octahedron and in the $(Ba^{\oplus\oplus})_3(Li^{\oplus})_3$ prismane. The next was the hexameric sodium salt of tetraphenoxiimidodiphosphate crystallized from toluene solution[37b], in which the $[Na_6^{\oplus}(O^{\delta\ominus})_{12}]$ cluster core is surrounded by a lipophilic skin with 24 phenyl rings on its outside, which permits dissolving of the "inorganic salt" in nonpolar solvents. In addition, by employing the well-established statistics based on the centroid/centroid distances of the phenyl substituents and the dihedral angles between them, the rather small

FIG. 28
Single crystal structure of the hexameric sodium (tetraphenoxy)imidodiphosphate with a $[Na_6^{\oplus}O_{12}]^{6\oplus}$ core and altogether 24 phenyl substituents on the outside of its lipophilic periphery, which provide solubility in apolar solvents such as toluene and from which the rather small contribution of the hydrocarbon skin to the enthalpy of formation dominated by the Coulombic interactions $Na^{\oplus}\ldots O^{\delta\ominus}$ could be estimated (*cf.* text)

contribution of the lipophilic skin of about 50 kJ mol^{-1} to the enthalpy of formation could be estimated, which is predominantly due to the Coulombic interactions $Na^{\oplus}\ldots O^{\delta\ominus}$ within the cluster core and, according to quantum-chemical calculation based on the structural data, amounts to about 5 000 kJ mol^{-1}. Summarizing, lipophilically wrapped polyion aggregates are formed due to the thermodynamic stability of the cluster core and their hydrocarbon skin supplies both kinetic shielding and the solubility in nonpolar solvents such as hexane[37].

Numerous other lipophilically wrapped polyion aggregates could be crystallized and structurally characterized in the meantime[37c,e] and others containing transition metal ions and sulfur as well as selenium ligands[38a] or alkali metal cations without[38b] or with oxygen ligands[38c] have been found in the literature – with many more presumably registered in the Cambridge Structural Database. Those that can be crystallized from solution add to the phenomenon of self-recognition and self-assembly of molecules currently being studied world-wide[36]. Evidently, inorganic salts with spatially partly shielding organic ligands (Figs 27 and 28) are formed readily due to their thermodynamically favourable cluster core and they could possibly be designed in the future according to precalculated interactions and optimum arrangements within the molecular state model presented, although their crystal packing cannot yet be predicted[28].

For the sake of illustration and because of its potential relevance to protein structures in NaCl-containing solutions, another and completely different lipophilically wrapped

FIG. 29

Single crystal structure of the tetrachloride–octahydrate aggregate in the intermolecular cavity of four protonated 2,4,6-tripyridine-1,3,5-triazine cations showing a variety of different hydrogen bonds such as $N^{\oplus}H\ldots O$, $N\ldots HO$ and $N^{\oplus}H\ldots Cl^{\ominus}$ fixing the cluster core to the cavity as well as $OH\ldots Cl^{\ominus}$ and $OH\ldots O$ within the core connecting the four $Cl^{\ominus}$ anions by $Cl^{\ominus}\ldots HOH\ldots Cl^{\ominus}$ and $Cl^{\ominus}\ldots HOH\ldots HOH\ldots Cl^{\ominus}$ subunits (*cf.* text)

polyion aggregate is depicted (Fig. 29): The tetrachloro-octahydrate in the intermolecular cavity of four protonated 2,4,6-tripyridine-1,3,5-triazine cations exhibits a complex hydrogen-bonded network, which is currently being analyzed by density functional calculations[30] based on the experimentally determined structural data.

5. SUMMARY AND FUTURE PROSPECTS

The essence of the molecular state approach for the preparative chemist (Figs 8 and 9), based on the topology (Fig. 10), the symmetry (Fig. 11), the effective nuclear potentials (Fig. 12) and the electron distribution (Fig. 13) and including the structure ↔ energy relation coupled by molecular dynamics (Chapter 2.3) can be summarized by a view of the periodic table of the elements through a magnifying glass revealing various properties of the molecules synthesized, characterized and reacted daily in the laboratory (Fig. 30): "What will one profit from looking at molecular states?" The multi-faceted examples selected from our own investigations and illustrating the usefulness of the molecular state fingerprints recorded in instrumental analysis as well as of quantum-chemical calculations at various levels of sophistication suggest "more, presumably, than can be imagined" (Fig. 30).

Future prospects for the molecular state approach, which greatly assists in explaining the properties of molecules, their microscopic reaction pathways and also interactions

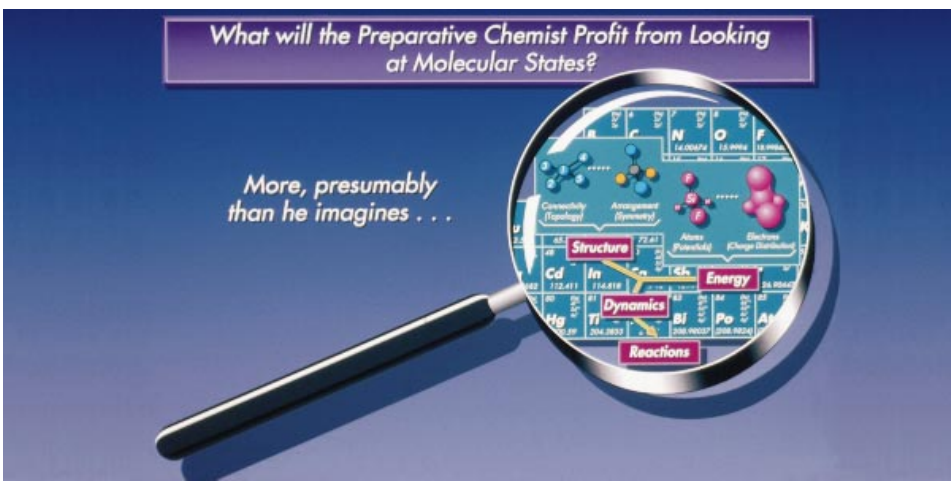

FIG. 30
Periodic table of the elements examined by a simplifying molecular state magnifier for the chemist emphasizing topology, symmetry, effective nuclear potentials and electron distribution as essential facets of molecules, and, above all, the structure ↔ energy relation coupled by molecular dynamics, which help to elucidate molecular properties, microscopic pathways of reductions and also dominant interactions in molecular crystals (*cf.* text)

in and between molecules in their crystals, are promising, especially in connection to future advances: First, the computer, an indispensable tool in modern chemistry, its calculation speed and its memory capacity are increasing at a breath-taking pace, and the progress in software development can be exemplified by the rapidly spreading use of density functional calculations. In addition, novel methods of measurement are added every year to the armory of physics. Unavoidably, these developments will broaden the applicability of molecular state models and, thereby, remove some of their present weaknesses such as the handling of multidimensional $3N - 6$ degrees of molecular freedom. Potential targets for investigations are like "fishes in the ocean" of chemistry and range from the design of ever more sophisticated experiments aimed at novel materials and processes to increasing insight into complex geochemical equilibria networks or the functions of biochemical macrosystems such as receptor sites or protein folding.

In conclusion, however, it must be pointed out that, in all probability, there will be always more questions than answers, or as stated in the foreword of a Ph.D. Thesis at the University of Frankfurt "actually, everything is more complicated".

The superb contributions of competent and highly motivated coworkers are deeply appreciated. The slides have been designed by R. Utermark, Hoechst Corporation.

REFERENCES

1. Preceding Reviews: a) Bock H.: *Molecular States and Molecular Orbitals*. Angew. Chem. *89*, 631–655 (1977); Angew. Chem., Int. Ed. Engl. *16*, 613–637 (1977); b) Bock H.: *Fundamentals of Silicon Chemistry: Molecular States of Silicon-Containing Compounds.* Angew. Chem. *101*, 1659–1682 (1989); Angew. Chem., Int. Ed. Engl. *28*, 1627–1650 (1989); c) Bock H.: *Principles of Phosphorus Chemistry: Molecular States of Phosphorus Compounds*. Phosphorus Sulfur Silicon *49/50*, 3–53 (1990); d) Bock H., Ruppert K., Nather C., Havlas Z., Herrmann H.-F., Arad C., Gobel I., John A., Meuret J., Nick S., Rauschenbach A., Seitz W., Vaupel T., Solouki B.: *Distorted Molecules: Perturbation Design, Preparation and Structures.* Angew. Chem. *104*, 564–595 (1992); Angew. Chem., Int. Ed. Engl. *31*, 550–581 (1992); e) Bock H.: *Molecular States of Sulfur Compounds in the Gas Phase, in Solution and in Crystals.* Phosphorus Sulfur Silicon *93/94*, 165–214 (1994).
2. *Cf. e.g.* Krafft F.: Angew. Chem. *81*, 634 (1969); Angew. Chem., Int. Ed. Engl. *8*, 660 (1969).
3. *Cf. e.g.* Neufeld S.: *Chronologie Chemie 1800–1980*, 2nd ed. VCH, Weinheim 1987.
4. *Cf. e.g. Electron Spectroscopy*, Vols 1–5 (C. R. Brundle and A. D. Baker, Eds). Academic Press, London 1977–1984.
5. *Cf. e.g.* Kurreck H., Kirste B., Lubitz W.: *Electron Nuclear Double Resonance Spectroscopy of Radicals in Solution – Application to Organic and Biological Chemistry*. VCH, Weinheim 1988.
6. Bock H.: *Ph.D. Thesis.* University of Munich, Munich 1958.
7. Bock H., Rudolph G., Baltin E., Kroner J.: *Colour and Constitution of Azo Compounds*. Angew. Chem. *77*, 469–484 (1965); Angew. Chem., Int. Ed. Engl. *4*, 457–471 (1965).
8. a) Bock H., Kompa K.-L.: Z. Anorg. Allg. Chem. *332*, 238 (1964); b) Bock H., Kompa K. L.: Angew. Chem. *74*, 327 (1962); Angew. Chem., Int. Ed. Engl. *1*, 264 (1962); c) Bock H., Kompa

K.-L.: Angew. Chem. *77*, 807 (1965); Angew. Chem., Int. Ed. Engl. *4*, 783 (1965); *cf.* also Chem. Ber. *99*, 1347, 1357, 1361 (1966).

9. a) Bock H., Kompa K.-L.: Angew. Chem. *78*, 114 (1966); Angew. Chem., Int. Ed. Engl. *5*, 123 (1966); b) Bock H., tom Dieck H.: Z. Naturforsch., B *21*, 739 (1966); c) Bock H., tom Dieck H.: Angew. Chem. *78*, 549 (1966); Angew. Chem., Int. Ed. Engl. *5*, 520 (1966); d) Bock H.: Angew. Chem. *74*, 695 (1962); Angew. Chem., Int. Ed. Engl. *1*, 550 (1962); e) Bock H., tom Dieck H., Pyttlik H., Schmoller M.: Z. Anorg. Allg. Chem. *357*, 54 (1968).
10. Heilbronner E., Bock H.: *The HMO Model and its Application*, Vol. 1–3. Verlag Chemie, Weinheim 1968–1970; Japanese translation: Hirokawa, Tokyo 1973; English translation: Wiley, New York 1975/76; Chinese translation: University Press, Kirin 1983.
11. a) Bock H., Ramsey B. G.: *Photoelectron Spectra of Nonmetal Compounds and Their Interpretation by MO Models*. Angew. Chem. *85*, 773–792 (1973); Angew. Chem., Int. Ed. Engl. *12*, 734–752 (1973); b) Wittel K., Bock H.: *Photoelectron Spectra of Organic Halogen Compounds* in *The Chemistry of Functional Groups* (S. Patai and Z. Rappoport, Eds), pp. 1499–1603. Wiley, Chichester 1983 (406 references cited therein); e) Stafast H., Bock H.: *Photoelectron Spectra of Cyano Compounds* in *The Chemistry of Functional Groups* (S. Patai and Z. Rappoport, Eds), pp. 137–185. Wiley, Chichester 1983 (113 references cited therein); d) Bock H., Solouki B.: *Photoelectron Spectra of Silicon Compounds* in *The Chemistry of Organic Silicon Compounds* (S. Patai and Z. Rappoport, Eds), pp. 555–653. Wiley, Chichester 1989 (252 references cited therein); e) Bock H., Solouki B.: *Organosilicon Radical Cations*. Chem. Rev. *95*, 1161–1190 (1995).
12. Bock H., Kaim W.: *Organosilicon Radical Cations*. Acc. Chem. Res. *15*, 9 (1982).
13. Bock H., Dammel R., Roth B.: *Molecular State Fingerprints and Semiempirical Hypersurface Calculations: Useful Correlations to Track Short-Lived Molecules* in *Rings, Clusters and Polymers of the Main Group Elements* (A. H. Cowley, Ed.). ACS Symp. Ser. *232*, 139–165 (1983).
14. a) Bock H., Solouki B.: *Photoelecton Spectra and Molecular Properties: Real-Time Gas Analysis in Flow Systems*. Angew. Chem. *93*, 425–442 (1981); Angew. Chem., Int. Ed. Engl. *20*, 427–444 (1981); b) Bock H., Solouki B., Aygen S., Bankmann M., Breuer O., Dammel R., Dorr J., Haun M., Hirabayashi T., Jaculi D., Mintzer J., Mohmand S., Muller H., Rosmus P., Roth B., Wittmann J., Wolf H. P.: *Optimization of Gas-Phase Reactions Using Real-Time PES-Analysis: Short-Lived Molecules and Heterogeneously Catalyzed Processes*. J. Mol. Spectrosc. *173*, 31–49 (1988).
15. Bock H., Dammel R.: *The Pyrolysis of Azides in the Gas Phase*. Angew. Chem. *99*, 518–540 (1987); Angew. Chem. Int. Ed. Engl. *26*, 504–526 (1987).
16. a) Bock H.: *Reaction of Carbon and Organosilicon Compounds as Viewed by a Preparative Chemist*. Rev. L'Actualité, Chim. *3*, 33 (1986); b) Bock H.: *Wie reagieren Moleküle mittlerer Grösse? Erzeugen, Nachweisen und Abfangen kurzlebiger Verbindungen*. Akademie der Wissenschaften und der Literatur Mainz, Abh. Math.-Naturw. Klasse *2*, 1–35 (1986); c) Bock H.: *What do we Actually Know About Reaction Pathways?* Polyhedron *7*, 2492 (1988).
17. a) *Cf.* ref.[1d]; b) Bock H.: *Some Static Aspects of Molecular Self-Organization from Single Crystal Structure Data*. Mol. Cryst. Liq. Cryst. *240*, 155–168 (1994); c) Bock H.: *Novel Hydrogen-Bridged Molecular Aggregates: Design, Structures and Potential Calculations*. Phosphorus Sulfur Silicon *87*, 23–29 (1994); d) Bock H.: *Was kristallisiert Wie und Warum? Statische Aspekte Molekularer Selbstorganisation aus Einkristall-Strukturdaten*. Akademie der Wissenschaften und der Literatur Mainz, Abh. Math.-Naturw. Klasse *1*, 1–59 (1995).
18. a) Reviews: Winnewisser M.: Chemie in unserer Zeit *18*, 1–16, 54–61 (1984) or Harju J., Sahn M., Henkel C., Wilson T. L., Sahn K. C., Pottasch S. R.: Astron. Astrophys. *223*, 197 (1990); b) Zanathy L., Bock H., Lentz D., Preugschat D., Botschwina P.: J. Chem. Soc., Chem. Commun. *1992*, 403.

19. Bock H., Gharagoozlo-Hubmann K., Nather C., Nagel N., Havlas Z.: Angew. Chem. *108*, 720 (1996); Angew. Chem., Int. Ed. Engl. *35*, 631 (1966).
20. a) Bock H., Mohmand S., Hirbayashi T., Semkow A.: Chem. Ber. *115*, 1339 (1982); J. Am. Chem. Soc. *104*, 312 (1982); b) Bock H., Ensslin W.: Angew. Chem. *83*, 435 (1971); Angew. Chem., Int. Ed. Engl. *10*, 404 (1971); c) Bock H., Ensslin W., Feher F., Freund R.: J. Am. Chem. Soc. *96*, 668 (1976); d) Bock H., Rohn G.: Helv. Chim. Acta *74*, 1221 (1991) and *75*, 160 (1992).
21. a) Bock H., Ried W., Stein U.: Chem. Ber. *114*, 673 (1981); b) Beagley B., Ulbrecht V., Katsumata S., Lloyd D. R., Connor J. A., Hudson G. A.: J. Chem. Soc., Faraday Trans. 2 *73*, 1278 (1977).
22. Bock H., John A., Havlas Z., Bats J. W.: *The Triplet Biradical Tris(3,5-di(t-butyl)-4-oxophenylene)methane: Crystal Structure, Spin and Charge Distribution*. Angew. Chem. *105*, 416 (1993); Angew. Chem., Int. Ed. Engl. *32*, 416 (1993).
23. Bock H., Stein U., Semkow A.: Chem. Ber. *113*, 3208 (1980).
24. Review: Zewail A.: *Femtochemistry*. J. Phys. Chem. *97*, 12427–12446 (1993).
25. a) Bock H., Hierholzer B., Vogtle F., Hollmann G.: *Radical Anion Substituted Crown Ethers as Cages for Metal Cations*. Angew. Chem. *96*, 74 (1984); Angew. Chem., Int. Ed. Engl. *23*, 57 (1984); b) Bock H., Jaculi D.: *Oxidation Reactions with Naked Permanganate Ions Under Aprotic Conditions*. Angew. Chem. *96*, 298 (1984); Angew. Chem., Int. Ed. Engl. *23*, 305 (1984); c) Bock H., Herrmann H.-F.: *[(Benzoquinone-18-crown-6)$^{\bullet}$Li^{+}Na^{+}]‡; a Paramagnetic Triple Ion with the Different Counter Cations*. J. Am. Chem. Soc. *111*, 7622 (1989); New J. Chem. *16*, 29 (1992); d) Bock H., Hanel P., Herrmann H.-F.: *ESR/ENDOR-Untersuchungen an Radikalanionen und Kontaktionenpaaren der Naturstoff-Chinone Mytomycin C, Streptonigrin, Entobex und 10,11-Dioxobrucin*. Z. Naturforsch., B *47*, 533 (1992); e) Bock H., John A., Kleine M., Nather C., Bats J. W.: *Die Einelektronen-Reduktion von Tetraphenyl-p-benzochinon mit Alkalimetallen: ENDOR-Spektren von Kontaktionenpaaren sowie Tripelionen in Lösung und Einkristallstrukturen der Neutralverbindung und ihres Natrium-Salzes*. Z. Naturforsch., B *49*, 529 (1994).
26. a) Bock H., Hierholzer B., Schmalz P.: Angew. Chem. *99*, 811 (1987); Angew. Chem., Int. Ed. Engl. *26*, 791 (1987); b) Bock H., Herrmann H.-F., Fenske D., Goesmann H.: Angew. Chem. *100*, 1125 (1988); Angew. Chem., Int. Ed. Engl. *27*, 1067 (1988).
27. Bock H., Gobel I., Havlas Z., Liedle S., Oberhammer H.: Angew. Chem. *103*, 193 (1991); Angew. Chem., Int. Ed. Engl. *30*, 187 (1991).
28. *Cf. e.g.* Wolff J. J.: *Crystal Packing and Molecular Geometry*. Angew. Chem. *108*, 2339 (1996); Angew. Chem., Int. Ed. Engl. *35*, 2195 (1996); and references therein.
29. a) Bock H., Ruppert K., Fenske D.: Angew. Chem. *101*, 1717 (1989); Angew. Chem., Int. Ed. Engl. *28*, 1685 (1989); b) Bock H., Ruppert K., Merzweiler K., Fenske D., Goesmann H.: Angew. Chem. *101*, 1075 (1989); Angew. Chem., Int. Ed. Engl. *28*, 1684 (1989); c) Bock H., Ruppert K., Havlas Z., Fenske D.: Angew. Chem. *102*, 1095 (1990); Angew. Chem., Int. Ed. Engl. *28*, 1042 (1990).
30. a) Bock H., Hauck T., Nather C., Rosch N., Staufer M., Haberlen O. D.: Angew. Chem. *107*, 1439 (1995); Angew. Chem., Int. Ed. Engl. *34*, 1353 (1995); b) Bock H., Havlas Z., Rauschenbach A., Nather C., Kleine M.: J. Chem. Soc., Chem. Commun. *1996*, 1529.
31. *Cf. e.g.* a) *Organic Solid State Chemistry* (G. R. Desiraju, Ed.). Elsevier, Amsterdam 1987; b) Desiraju G. R.: *Crystal Engineering*. Elsevier, Amsterdam 1989; c) Jeffrey G. A., Saenger W.: *Hydrogen Bonding in Biological Structures*. Springer, Berlin 1991; d) *Structure Correlation* (H. B. Burgi and J. D. Dunitz, Eds), Vols 1 and 2. VCH, Weinheim 1994.
32. *Cf. e.g.* a) Bock H., Nather C., Havlas Z.: J. Am. Chem. Soc. *117*, 3869 (1995); b) Bock H., Nather C., Havlas Z., John A., Arad C.: Angew. Chem. *106*, 931 (1994); Angew. Chem., Int. Ed.

Engl. *33*, 875 (1994); c) Bock H., Gharagozloo-Hubmann K., Nather C., Nagel N., Havlas Z.: Angew. Chem. *108*, 720 (1996); Angew. Chem., Int. Ed. Engl. *35*, 631 (1996).

33. Cf. e.g. a) Bock H., Vaupel T., Nather C., Ruppert K., Havlas Z.: Angew. Chem. *104*, 348 (1992); Angew. Chem., Int. Ed. Engl. *31*, 299 (1992); b) Bock H., Dienelt R., Schodel H., Havlas Z., Herdtweck E., Hermann W. A.: Angew. Chem. *105*, 1826 (1993); Angew. Chem., Int. Ed. Engl. *32*, 1758 (1993); c) Bock H., Dienelt R., Schodel H., Havlas Z.: J. Chem. Soc., Chem. Commun. *1993*, 1792.
34. Cf. e.g. a) Bock H., Seitz W., Sievert M., Kleine M., Bats J. W.: Angew. Chem. *108*, 2382 (1996); Angew. Chem., Int. Ed. Engl. *35*, 2244 (1996) and references to other publications; b) Bock H., Rauschenbach A., Nather C., Kleine M., Havlas Z.: Liebigs. Anal. *1996*, 2185; cf. also ref.[30b]; c) Bock H., Seibel A., Kleine M., Nagel N., Havlas Z.: Unpublished results.
35. Cf. e.g. a) Bock H., Meuret J., Ruppert K.: Angew. Chem. *105*, 413 (1993); Angew. Chem., Int. Ed. Engl. *32*, 415 (1993); J. Organomet. Chem. *445*, 19 (1993); b) Bock H., Gobel I., Nather C., Havlas Z., Gavezzotti A., Filippini G.: Angew. Chem. *105*, 1823 (1993); Angew. Chem., Int. Ed. Engl. *32*, 1755 (1993); c) Schodel H., Nather C., Bock H., Butenschon F.: Acta Crystallogr., B *52*, 842 (1996).
36. Cf. e.g. a) Lehn J. M.: *Supramolecular Chemistry*. VCH, Weinheim 1995; cf. also Angew. Chem. *102*, 1347–1361 (1991); Angew. Chem., Int. Ed. Engl. *30*, 1304–1319 (1991); b) Lahav M., Leiserowitz L., Kjaer K., Als-Nielsen J., Jacquemain D., Wolf S. G., Leveiller F., Deutsch M.: Angew. Chem. *104*, 134–158 (1992); Angew. Chem., Int. Ed. Engl. *31*, 130–154 (1992). c) Belohradsky M., Raymo F. M., Stoddard J. F.: Collect. Czech. Chem. Commun. *61*, 1–43 (1996); d) *cf*. also ref.[35a].
37. Lipophilically wrapped polyion aggregates, crystallized and struturally characterized by the Frankfurt group: a) $\{[(Ba^{2+})_6(Li^+)_3(O^{2-})_2]^{11+}(^-O–C(CH_3)_3)_{11}(OC_4H_8)_3\}$: Bock H., Hauck T., Nather C., Rosch N., Staufer M., Haberlen O. D.: Angew. Chem. *107*, 1439 (1995); Angew. Chem., Int. Ed. Engl. *34*, 1353 (1995); b) $\{[OP–N^-–PONa^+]_6(C_{144}H_{120}O_{24})\}$: Bock H., Schodel H., Havlas Z., Herrmann E.: Angew. Chem. *107*, 1441 (1995); Angew. Chem., Int. Ed. Engl. *34*, 1355 (1995); c) $\{[(Li^+)_6(NH_3)_2(O^-)_6](C_{88}H_{110}O_2)\}$: Bock H., John A., Nather C., Havlas Z.: J. Am. Chem. Soc. *117*, 9367 (1995); d) $\{[(K^+)_6(O_{12})^{6-}](C_{102}H_{80}N_6)\}$: Bock H., Dienelt R., Schodel H., Havlas Z.: Tetrahedron Lett. *36*, 7855 (1995); e) $\{[(Li^+)_4(O^-)_4](C_{96}H_{84}O_{10}Si_8)\}$, $\{[(Na^+)_4(O^-)_4](C_{96}H_{84}O_6Si_8)\}$, $\{[(K^+)_4(O^-)_4(C_{72}H_{60}Si_4)\}$ as well as $\{[(Li^+)_4(O^-)_4](C_{64}H_{76}O_4Si_4)\}$: Bock H., Ansari M., Nagel N., Havlas Z.: Unpublished results.
38. Cf. e.g. a) Fenske D., Longoni G., Schmid G. in: *Clusters and Colloids – From Theory to Applications* (G. Schmid, Ed.), pp. 89–298. VCH, Weinheim 1994; b) Simon A.: Struct. Bonding (Berlin) *36*, 81 (1979); c) Weiss E.: Angew. Chem. *105*, 1565 (1993); Angew. Chem., Int. Ed. Engl. *32*, 1501 (1993).